

Carbon-Based Photothermal Actuators

Bing Han, Yong-Lai Zhang,* Qi-Dai Chen, and Hong-Bo Sun*

Actuators that can convert environmental stimuli into mechanical work are widely used in intelligent systems, robots, and micromechanics. To produce robust and sensitive actuators of different scales, efforts are devoted to developing effective actuating schemes and functional materials for actuator design. Carbon-based nanomaterials have emerged as preferred candidates for different actuating systems because of their low cost, ease of processing, mechanical strength, and excellent physical/chemical properties. Especially, due to their excellent photothermal activity, which includes both optical absorption and thermal conductivities, carbon-based materials have shown great potential for use in photothermal actuators. Herein, the recent advances in photothermal actuators based on various carbon allotropes, including graphite, carbon nanotubes, amorphous carbon, graphene and its derivatives, are reviewed. Different photothermal actuating schemes, including photothermal effect-induced expansion, desorption, phase change, surface tension gradient creation, and actuation under magnetic levitation, are summarized, and the light-to-heat and heat-to-work conversion mechanisms are discussed. Carbon-based photothermal actuators that feature high light-to-work conversion efficiency, mechanical robustness, and noncontact manipulation hold great promise for future autonomous systems.

1. Introduction

Inspired by natural autonomous systems that can change their shape and appearance under external stimuli,^[1–6] artificial smart devices enabling the direct conversion of various environmental stimuli (e.g., heat,^[7,8] solvent,^[9,10] light,^[11–13] electric,^[14,15] magnetism,^[16,17] and moisture)^[18,19] into mechanical work have been successfully developed for cutting-edge applications including micro-electromechanical systems (MEMS),^[20,21]

microrobotics,^[16,22–25] micromachines,^[26–28] sensors,^[29–31] to camouflage surfaces.^[32,33] The design and fabrication of multifarious actuators have emerged as a promising research field. To achieve fast, sensitive, and large deflection actuators, considerable efforts have been devoted to developing advanced actuation strategies and various stimuli-responsive materials/structures.

Among the different types of actuating schemes, light-driven strategies that enable remote control of actuators are promising because they do not require complex coupled instruments and can be freely manipulated in a noncontact manner.^[4,13,15,34,35] Moreover, light is a clean and safe energy source with easily switchable properties. Precise light manipulation can be realized by controlling various parameters such as the light intensity, wavelength, spot radius, exposure duration, and polarization direction. Because of these unique advantages, light-driven actuators have great potential for a wide range of applications.^[12,36–38] Generally, light-driven strategies can be classified into different categories according to their mechanism, such as

optical tweezer manipulation, and photothermal and photochemical actuation.^[39–46] Among these light-driven strategies, photothermal actuation emerges as an appealing manner since it can be realized through various photothermal effects (e.g., expansion of volume, desorption of molecules, phase change, and surface tension effects). Moreover, as compared with other light-driven actuators, photothermal actuators usually have a relatively simple design principle, outstanding performance, controllable reconfiguration, and good stability. To make a robust photothermal actuator, appropriate photothermal materials with high light absorption and good thermal conductivity are required so that the photon energy can be effectively converted into heat energy, inducing the mechanical deformation.^[42,47–49]

Carbon-based nanomaterials are superior candidates for photothermal applications. Based on the different bonding behaviors of carbon atoms, the carbon material family can be generally classified into i) graphite, carbon nanotube and graphene with entire sp^2 hybrid bonds, ii) amorphous carbon with sp^2 and sp^3 hybrid bonds, iii) diamond with pure sp^3 hybrid bonds, and iv) carbon chain with sp hybrid bonds.^[50–52] These carbon allotropes have unique merits including remarkable optical, thermal, and mechanical properties, which is promising for actuator design.^[53,54] Most carbon materials are photothermally active and possess wideband optical absorption that permits absorption of light of various wavelengths,

B. Han, Prof. Y.-L. Zhang, Prof. Q.-D. Chen
State Key Laboratory of Integrated Optoelectronics
College of Electronic Science and Engineering
Jilin University
2699 Qianjin Street, Changchun 130012, China

E-mail: yonglaizhang@jlu.edu.cn

Prof. H.-B. Sun
State Key Laboratory of Precision
Measurement Technology and Instruments
Department of Precision Instrument
Tsinghua University
Haidian district, Beijing 100084, China
E-mail: hbsun@tsinghua.edu.cn

 The ORCID identification number(s) for the author(s) of this article can be found under <https://doi.org/10.1002/adfm.201802235>.

DOI: 10.1002/adfm.201802235

and most have high photothermal conversion efficiencies.^[55–58] With excellent thermal conduction characteristics, carbon materials can transfer the as-obtained thermal energy to the heat-sensitive materials, achieving effective photothermal actuation.^[59,60] In addition, carbon materials have many advantages, such as excellent physical and chemical stability, high mechanical strength, conductivity, as well as tunable light absorption properties, which allow for broad application of carbon-based actuators.^[61]

In this review, we focus on the recent advancements in carbon-based photothermal actuators and highlight their unique advantages, good performance, and potential for future applications. Specific light-to-heat conversion mechanisms and strategies that enable photothermal actuation are discussed. The performance of various photothermal actuators focusing on energy conversion, response/recover time, stability, mechanical strength, and actuating manners has been reviewed in details. **Figure 1** shows a summary of typical actuators constructed of different carbon-based materials and their possible light-to-work mechanisms, including photothermal expansion, desorption, phase change, Marangoni effect, and magnetic susceptibility change. In addition, the advantages and limitations of carbon-based photothermal actuators and the current challenges in this field are discussed in Section 4. The development of carbon-based photothermal actuators may stimulate rapid progress in various smart devices for cutting-edge applications.

2. Carbon-Based Materials for Photothermal Actuator Design

Carbon materials such as carbon nanotubes (CNTs), graphene, graphite, and amorphous carbon have been recognized as the most efficient photothermal materials.^[62–64] They have been widely used and investigated because of their low cost and abundance.^[50,65,66] In the development of photothermal actuators, choosing appropriate photothermal materials that can realize efficient light-to-heat conversion is essential.^[30,42,67] Light carries photons energy propagating along the direction of electromagnetic radiation. When light interacts with carbon materials, the photon energy can be absorbed if it is higher than the optical bandgap, leading to the photoexcitation of electrons. The energy of the excited electrons is transferred to the lattice by electron–phonon coupling, which produces heat. Generally, the thermal conduction is transported through acoustic phonons and electrons. However, in carbon materials, phonons account for most of the heat conduction. Diamond, graphene, and CNTs possess excellent thermal conductivity because heat is dominated by the intrinsic properties of the perfect sp^3 or sp^2 lattice.^[51,68,69] In amorphous carbon, the thermal energy is greatly affected by phonon scattering on boundaries or by disorder. Various types of carbon materials have been employed for actuator design because of their excellent photothermal properties. Carbon materials can be functionalized as a solo photothermal layer or used as nanofillers in hybrid materials, offering opportunities to enhance the photothermal and mechanical properties of various devices.^[70] **Figure 2** shows the structures of several typical carbon materials and their thermal properties. An overview of different carbon allotropes showing



Bing Han received her B.S. degree from the College of Electronic Science and Engineering (2012), Jilin University. She is currently a Ph.D. student in the State Key Laboratory of Integrated Optoelectronics, Jilin University. Her research work focused on graphene and graphene-based composite materials. Her current research interests include laser printed graphene devices, applications of graphene materials in optical detection, and light-driven bioinspired robots.



Yong-Lai Zhang received his B.S. degree (2004) and Ph.D. degree (2009) from Jilin University, China. In 2010, he joined the faculty in the State Key Laboratory of Integrated Optoelectronics, College of Electronic Science and Engineering, Jilin University. In 2011, he worked as a Research Professor in Yonsei University, Republic of Korea. After that, he was awarded a “Hong Kong Scholar” postdoctoral fellowship and worked at the Center of Super Diamond and Advanced films (COSDAF), City University of Hong Kong. His research interests include laser micro-nanofabrication of functional micro-nanostructures, smart actuators, and Bio-MEMS.



Hong-Bo Sun received his Ph.D. degree in 1996 from Jilin University, China. He worked as a postdoctoral researcher at the University of Tokushima, Japan, from 1996 to 2000, and then as an assistant professor in Department of Applied Physics, Osaka University, from 2000 to 2006. From 2006, he worked as a Changjiang-Scholar Professor at Jilin University, and in 2017 he moved to Tsinghua University, China. His research focuses on laser micro-nanofabrication and their applications in micro-optics, micromachines, microfluids, and microsensors.

the physical and optical properties of commonly used carbon materials (including thermal conductivity, mechanical strength, specific surface area, and so on) is summarized in **Table 1**.

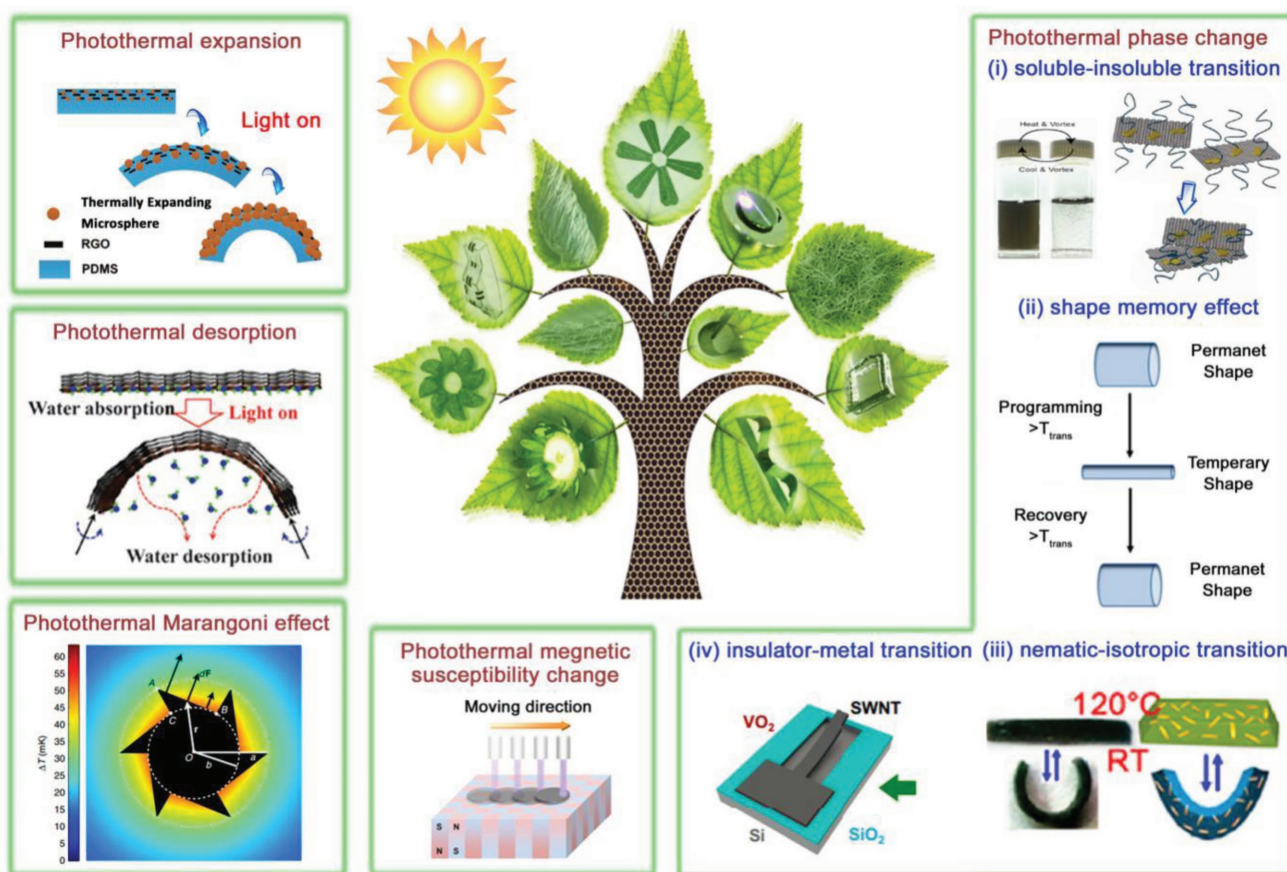


Figure 1. General concept of carbon-based photothermal actuators. For photothermal expansion image: reproduced with permission.^[123] Copyright 2017, WILEY-VCH; For photothermal desorption: reproduced with permission.^[102] Copyright 2015, American Association for the Advancement of Science; For photothermal Marangoni effect: reproduced with permission.^[17] Copyright 2015, Nature Publishing Group; For photothermal magnetic susceptibility change image: reproduced with permission.^[175] Copyright 2012, American Chemical Society; For soluble-insoluble transition: reproduced with permission.^[100] Copyright 2013, American Chemical Society; For shape memory effect: reproduced with permission.^[91] Copyright 2014, Springer International Publishing AG; For nematic-isotropic transition: reproduced with permission.^[166] Copyright 2016, American Chemical Society; For insulator-metal transition: reproduced with permission.^[171] Copyright 2017, American Association for the Advancement of Science; For image of sunflower: reproduced with permission.^[148] Copyright 2017, WILEY-VCH; For micro gear: reproduced with permission.^[173] Copyright 2017, WILEY-VCH; For origami assembly of a car: reproduced with permission.^[123] Copyright 2017, WILEY-VCH; For graphene fiber motor: reproduced with permission.^[128] Copyright 2015, WILEY-VCH; For biomimetic flower: reproduced with permission.^[110] Copyright 2016, WILEY-VCH; For rotary motion of PG disk: reproduced with permission.^[175] Copyright 2012, American Chemical Society; For SEM image of SWCNT membrane: reproduced with permission.^[181] Copyright 2015, American Chemical Society; For cubic frame: reproduced with permission.^[148] Copyright 2017, WILEY-VCH; For SEM image of RGO-CNT membrane: reproduced with permission.^[122] Copyright 2015, WILEY-VCH; For tubular CNT/polymer bilayer: reproduced with permission.^[76] Copyright 2017, WILEY-VCH.

2.1. Carbon Nanotubes

CNTs are considered as 1D carbon materials with cylindrical structures that have been widely adopted in photothermal actuators because of their outstanding physical properties, such as good light absorption property in the visible and near-infrared region,^[71] strong mechanical strength (1 TPa), and high thermal conductivity (up to $6000 \text{ W m}^{-1} \text{ K}^{-1}$).^[68,72,73,184–191] The outstanding light absorption capability can lead to an intense thermal accumulation, and thus a gain of sufficient heat energy for the subsequent actuation. Due to the excellent photothermal properties, actuators using a very small amount of CNTs as a photothermal layer can be actuated under light irradiation.^[74] CNTs have been widely recognized as efficient photothermal materials for various light-to-work conversion systems such

as photothermal effect-induced bending, twisting, volume changes, and even self-pulling.^[44] When CNTs are randomly assembled into a polymer matrix, the mechanical properties of the resultant composite materials such as the strength, stability, and stiffness can be significantly improved as compared with pure polymers.^[75] Therefore, CNT-based actuators usually exhibit large deflection, strong robustness, and a long lifetime. Recently, Hu et al. designed a robust jumping robot based on the rolled multiwalled CNT/polymer bilayer composite actuator.^[76] This robot showed remarkable performance mainly due to the conductivity brought by the loosely CNT network, good optical absorption of CNT, well CNT–polymer interfacial contact, and the distinct expansion degrees between the two layers.

Generally, CNTs are classified into two main categories: single-walled carbon nanotubes (SWCNTs) with a one-atom

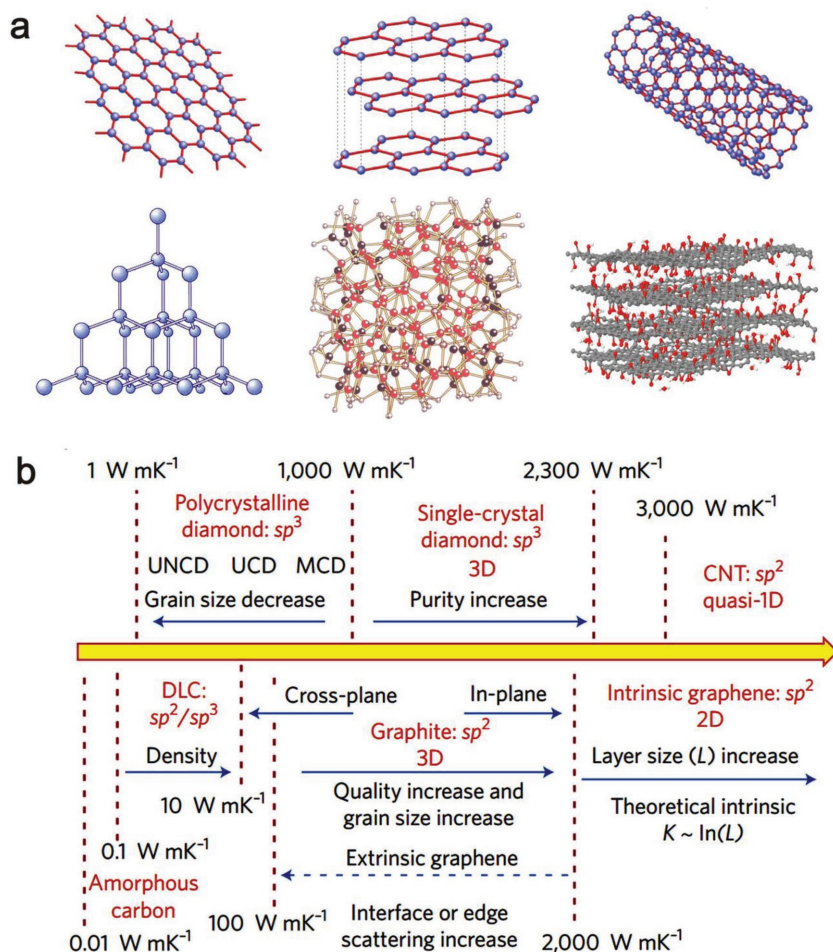


Figure 2. Lattice structure of typical carbon materials and their thermal properties. a) Structures of graphene, graphite, CNT, diamond, amorphous carbon, and GO. Structure of GO: Reproduced with permission.^[53] Copyright 2010, American Chemical Society. Structure of amorphous carbon: Reproduced with permission.^[115] Copyright 1993, the American Physical Society. b) Thermal conductivities of different carbon materials, varying over five orders of magnitude. Reproduced with permission.^[51] Copyright 2011, Springer Nature.

thickness and multiwalled carbon nanotubes (MWCNTs), which are formed by a number of concentric SWCNTs. SWCNTs can also be classified into different types because the honeycomb

structure of graphitic sheets can roll in different manners such as the zigzag, armchair, and chiral forms. The rolling up direction can be described in terms of a vector $C = na_1 + ma_2$, where a_1 and a_2 are the unit vectors, and n and m are indices. The properties of SWCNTs vary significantly with different (n, m) values. Consequently, SWCNTs that feature specific chirality may demonstrate wavelength-selective properties,^[77] whereas MWCNTs usually possess broadband adsorption due to the wide distribution of various chiralities. Recent advances in chirality purification of CNTs enable use of enriched single-chirality SWCNTs with strong and narrow optical absorptions, which may offer opportunities to design photothermal actuators with desirable wavelength-selective properties. Taking advantage of the intriguing photothermal properties of SWCNTs, Javey and co-workers presented a photoactuator device based on SWCNT/polymer bilayers using simple vacuum filtration.^[77] In their work, three types of SWCNTs were employed to tune the light absorption properties: i) high-pressure carbon monoxide disproportionation (HiPCO) SWCNTs (a mixture of different n, m); ii) metallic nanotubes with a single absorption peak at ≈ 700 nm ($|m - n| = 3k$, where k is an integer); and iii) single-chirality nanotubes with characteristic absorption peaks at ≈ 560 and 970 nm ($n = 6, m = 5$). The type-dependent SWCNTs served as excellent light absorbers and wavelength-sensitive mediums (Figure 3a–c). This special optical property allowed for actuators with monochromatic light-driven features.

CNTs that possess ultralarge length to diameter ratio have shown excellent mechanical flexibility along their axis.^[78] Therefore, the orientation of CNTs can greatly influence the density, mechanical strength, and deformation manner of actuators with CNTs embedded, which has a significant impact on

Table 1. Typical carbon allotropes and their physical/optical properties.

Material	Absorption characteristics	Thermal conductivity [W m ⁻¹ K ⁻¹]	Mechanical strength [TPa]	Specific surface area [m ² g ⁻¹]	Ref.
Carbon nanotube	–	1000–6000	0.063	50–1315	[184–187]
SWCNT	Chirality related	Up to 6000	1	435	[95,181,188]
MWCNT	–	2000–3000	0.2–4	25–260	[44,95,185,189]
ANT	Blackest material ($\approx 99.9\%$)	99.5	0.016	500	[184,190,191]
Graphene	Monolayer graphene absorb white light of $\approx 2.3\%$	Up to 6000	1	2630	[95,105,119,192,193]
GO	–	1	0.032	705	[95,131,192,194]
RGO	–	400–1800	0.042	466–1520	[195–199]
Graphite	–	3000	0.13	0.8–50	[185,200,201]
Carbon black	–	0.01	–	100	[51,202]

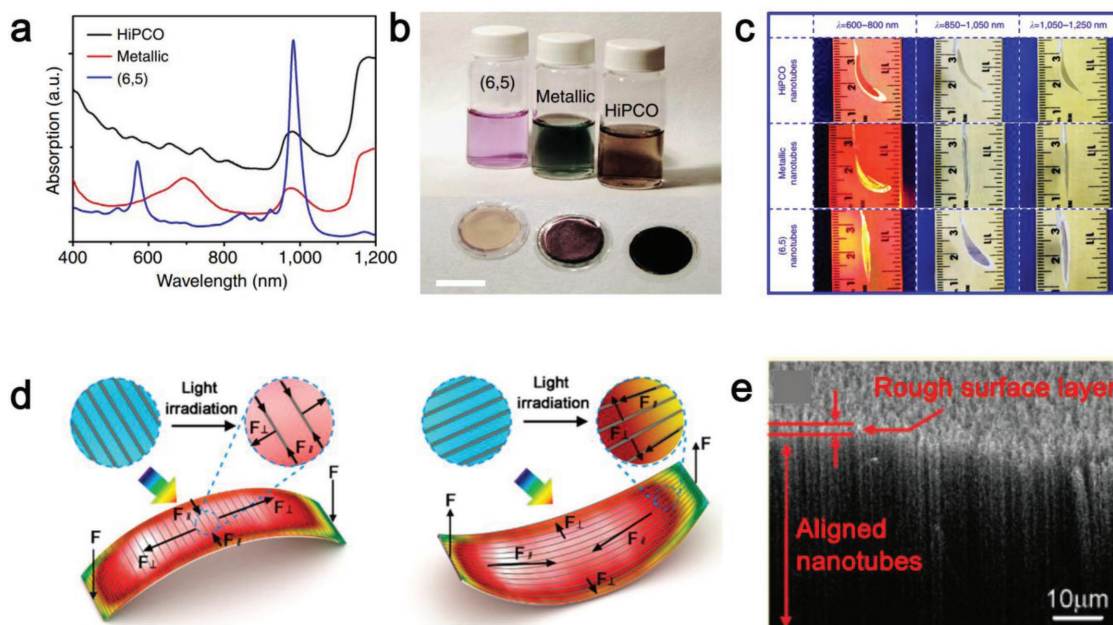


Figure 3. Illustration of a CNT-based actuator with unique properties. a) Optical absorption spectra for three types of nanotubes, HiPCO, metallic, and (6, 5)-enriched CNTs. b) Optical image of three CNT solutions and their corresponding actuator films. c) Wavelength-sensitive response. a–c) Reproduced with permission.^[77] Copyright 2014, Springer Nature. d) Schematic illustration of the different bending directions of actuators assembled with various nanotube arrangements. Reproduced with permission.^[79] Copyright 2016, American Chemical Society. e) Scanning electron microscopic (SEM) image of a VACNTs sample. Reproduced with permission.^[82] Copyright 2008, American Chemical Society.

modulating photothermal actuation. Traditional actuators constructed of randomly distributed CNTs often perform unpredictable bending. To address this issue, Peng and co-workers proposed a strategy that enables controllable deformations by embedding aligned carbon nanotubes (ACNTs) in photothermal actuators.^[79] The ACNTs are assembled by van der Waals forces and the resulting ACNT/paraffin wax and polyimide bilayer actuators retained the excellent properties of individual nanotubes.^[80] The bilayer strips with transverse and longitudinal arrangement of CNTs exhibited distinct types of actuation (Figure 3d). By manipulating the CNT alignment direction, several types of light-to-work actuations, including phototropic and apheliotropic bending and even helical twisting, have been realized. Upon irradiation, a transversely aligned strip exhibited a rapid bending performance toward the polyimide side whereas a longitudinally aligned strip bent toward the ACNT/paraffin wax side. This unusual phenomenon was because of the anisotropic properties of ACNTs (the longitudinal modulus is high whereas the transverse modulus is low), which caused a geometric constraint on the expansion of the paraffin wax. Thus, the paraffin wax tended to expand perpendicularly to the orientation of the ACNTs. Actuators with right-handed and left-handed helical deformation were realized through adjusting the angle between the longitudinal axis of the strip and the orientation of CNT alignment. Thus, the actuator performance could be controlled by programming the nanoscale structures.^[81]

To obtain better light harvesting capability, vertically aligned carbon nanotubes (VACNTs) that are reported to be the blackest material, with greater than 98% absorbance in a wide spectral range (from 200 nm to 200 μm), appear to be a good choice for producing photothermal actuators with high energy conver-

sion efficiency. VACNTs are carbon nanotubes oriented along their longitudinal axes normal to a substrate surface with a very high surface roughness (Figure 3e).^[82,83] The incident light can be trapped in the CNT forests due to the extremely low index of refraction, multiple reflections, and the nanoscale surface roughness. Using VACNTs as an outstanding photothermal layer, direct light-to-work conversion has been achieved based on the Marangoni effect (see Section 3.4).^[84]

As nanoscale energy sources, CNTs can absorb light in a wide spectral range and effectively convert it into heat, revealing great potential for developing photothermal actuators.^[85] CNTs also feature good mechanical strength, stability, and conductivity. These unique advantages make CNTs preferred photothermal materials for actuator design. However, the use of CNTs in actuators also suffers from several problems including chirality purification of CNTs, substrate transferring of CNTs arrays, and the integration of CNTs with actuator devices. With the progress of techniques for CNT preparation and processing, CNTs play an important role in various photothermal devices.

2.2. Graphene and Its Derivatives

As a new member of the carbon material family, graphene, a one-atom-thick 2D material with entire sp^2 hybrid bonds, has emerged as a potential reagent in material science.^[61,86–88] Because graphene has many exceptional physical properties, it has attracted considerable interests in various scientific fields including photothermal actuators.^[89–92] Notably, graphene has several advantages for photothermal actuator design, including i) high light absorption ability,^[57,93] ii) excellent mechanical

strength,^[54,94] iii) high thermal conductivity,^[95,192–199] iv) distinctively negative coefficient of thermal expansion (CTE), and v) ultralight weight. Because of the high photothermal conversion efficiency, graphene holds great promise in high-efficiency light energy utilization, photothermal therapy, and photothermal devices.^[96] To develop photothermal actuators, graphene that functionalizes as a photothermal layer is usually combined with other functional materials such as hydrogels, liquid crystals elastomers (LCEs), and shape memory polymers (SMPs) to form an asymmetric bilayer structure.^[6,97,98] Jiang et al. fabricated a soft rapid-response actuator with by combining a composite layer of polydimethylsiloxane (PDMS) and graphene nanoplates (GNPs, 5 wt%) with a pristine PDMS layer.^[99,205] The bilayer strip (7 mm × 1 mm) can be deflected ≈1500 μm within 3.4 s under NIR irradiation. Owing to the photothermal effect of graphene, a temperature increment of 60 °C at the PDMS/GNP layer was observed within 5 s. Under light irradiation, the phonons within graphene layer vibrate and interact with each other dramatically, exhibiting the accumulation of heat energy in a few seconds. Based on this light-to-heat conversion scheme, light-driven hydrogel-^[6,100,101] paper,^[15,90,102] and fiber-like^[103] graphene actuators have been developed.

In other carbon-based photothermal actuators, carbon materials are added to achieve fast light-to-heat conversion and high mechanical strength; however, transparency is sacrificed for high performance. Transparent actuators have been realized when a thin layer of graphene is used as a photothermal layer because of the ultrathin characteristics of graphene. As reported by Xu et al.,^[104] a transparent and ultrathin photothermal actuator based on monolayer graphene, polydopamine, and poly(*N*-isopropylacrylamide) (PNIPAAm) was successfully developed (Figure 4a). Although the functionalized graphene layer is only 5–10 nm thick, the self-folding actuators exhibit very good mechanical stiffness. Using a bilayer of large-area graphene and chitosan, Xie et al. fabricated an actuator that features visible-light transparency using monolayer graphene as functional material, allowing for the development of transparent humanoid robots and machines.^[87] However, in the case of photothermal actuation, the monolayer graphene may suffer from low photothermal conversion rate since transparent graphene monolayer has much lower light absorption of white light (≈2.3%) than those of bulk carbon materials.^[105] Nevertheless, the actuators based on monolayer graphene have realized rapid and large deformation, showing good mechanical robustness.

However, the use of pristine graphene is not easy. Problems in preparation of single-layer graphene and the dispersion of graphene sheets in solution for tractable processing usually restrict their application. Graphene is a hydrophobic mate-

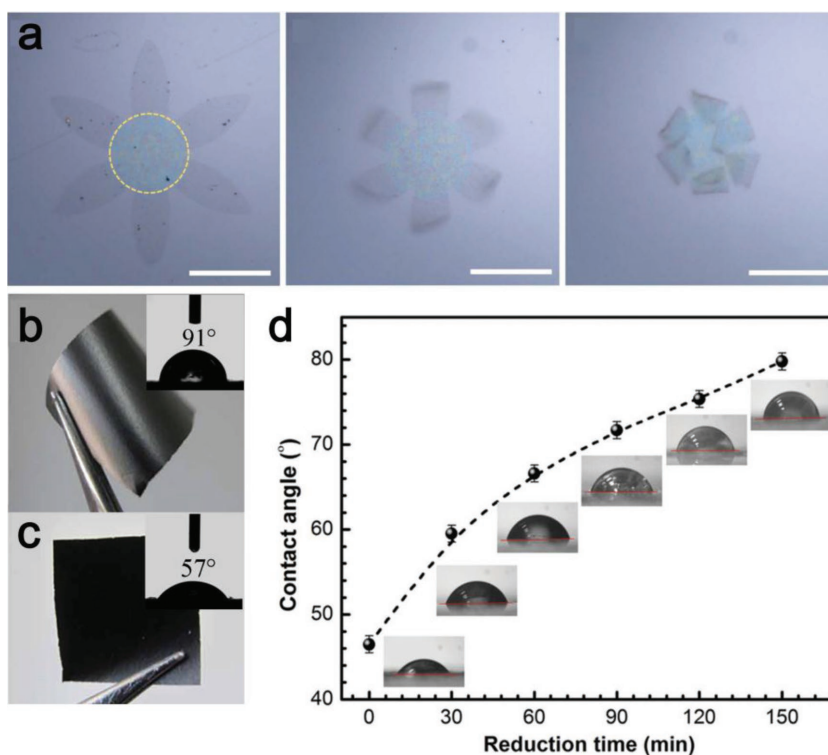


Figure 4. Graphene-related materials for actuator design. a) Optical microscope image of an ultrathin graphene actuator. Reproduced with permission.^[104] Copyright 2017, American Association for the Advancement of Science. b) Photograph of an RGO film and its contact angle measurement. c) Photograph of a GO film and its contact angle measurement. Reproduced with permission.^[182] Copyright 2015, Springer Nature. d) The relationship between the contact angle and the RGO film with different reduction times. Reproduced with permission.^[18] Copyright 2015, Wiley-VCH.

rial and is not soluble in most solvents.^[86] When graphene is mixed with polymer materials, precipitation often occurs. For actuators based on graphene composite materials, homogeneous dispersion of graphene in the polymer matrix is critical to achieve high performance. Chemical functionalization is a feasible and effective method of improving the dispersion of graphene in organic solvents. However, the damage to the sp² network must be considered because the defects severely affect the mechanical, thermal, and optical properties. A modified sulfonated graphene was reported to demonstrate good solubility in common organic solvents without destroying their integrity of graphitic network. Liang et al. incorporated sulfonated graphene into thermoplastic polyurethane (TPU) material and fabricated a remarkable light-triggered actuator with dramatically enhanced mechanical properties.^[106] Isocyanate-treated graphene also exhibits good dispersion in the polymer matrix but it often results in a damaged sp² network. The isocyanated graphene exhibits a poor response upon light irradiation.

Graphene oxide (GO) prepared by chemical oxidization of graphite and exfoliation in water reveals great potential for practical usage because it allows for mass production. Generally, GO can be considered oxygen group-functionalized graphene sheets. The presence of hydrophilic oxygen groups endows GO with good water dispersibility and makes GO different from graphene. To remove the oxygen groups and partially recover

the properties, reduction treatments such as thermal, chemical, and photoreduction are generally necessary.^[107] Making full use of the solution-processing capability of GO, reduced GO (RGO) sheets have been widely used as doping agents to develop photothermal composites. The RGO-based photothermal actuators possess mechanical strength and optical and thermal properties comparable to those made with pristine graphene material.^[108] Selective removal of the oxygen-containing group on GO enables precise control over the interaction between the water molecules and GO sheets, allowing for feasible moisture actuation.^[103,109] Because of the removal of hydrophilic oxygen groups, the RGO surface becomes hydrophobic (Figure 4b,c).^[182] The surface wettability of an RGO film can be modulated by controlling the reduction degree (Figure 4d).^[18] In a GO film, water molecules can easily be adsorbed, which induces swelling of the GO layer, whereas the swelling effect is not obvious in the RGO film. Therefore, the combination of GO and RGO forms moisture-responsive bilayer actuators. Because RGO is photothermally active and the absorption of water shows a strong temperature dependence, these moisture-responsive actuators can also be manipulated in a photothermal manner. This mechanism is introduced in detail in the photothermal desorption section.

2.3. Other Carbon-Based Materials

In addition to CNTs and graphene, other carbon materials, such as graphite and carbon black, have been used in photothermal actuators due to their excellent stability, low cost, easy accessibility, and ease of processing. Graphite is an opaque, black, thermodynamically stable carbon material.^[200,201] Because the in-plane carbon atoms are covalently bonded in a honeycomb lattice with three bonding sites satisfied, the fourth delocalized electrons are free to move throughout the plane within the graphite layers. Another unique feature of graphite is the weak van der Waal bonds formed between layers. The thermal property of graphite is anisotropic; phonons propagate quickly along the bonding planes whereas their travel from layer to layer is impeded. The weak interaction between layers enables the graphite material to be easily slid or separated, and graphite is soft enough to draw a streak on paper. Weng et al. presented a simple pencil-on-paper actuator that could be used in various conditions.^[110] The pencil and paper are both common materials that are low cost and easy to obtain. In their work, common pencils (10 B) were used to deposit graphite by drawing 1000 times onto a piece of paper. The colorful pencils can make multicolor actuators (Figure 5a). Graphite strongly absorbs light over a broad range extending from the UV to NIR wavelengths. Upon light irradiation, the actuator exhibited ultralarge actuation (curvature: 2.6 cm^{-1}). Applying this pencil-on-paper structure, a colorful biomimetic flower (Figure 5b) and smart curtain were made with obvious bending performance. However, graphite is not often used in a pure form as a standalone structural material because of its shear plane and brittle mechanical properties. When covalent bonds occur between the graphite layers, replacing the weak intermolecular forces, graphite becomes pyrolytic graphite (PG).^[111] The PG possesses a much higher thermal conductivity than graphite.

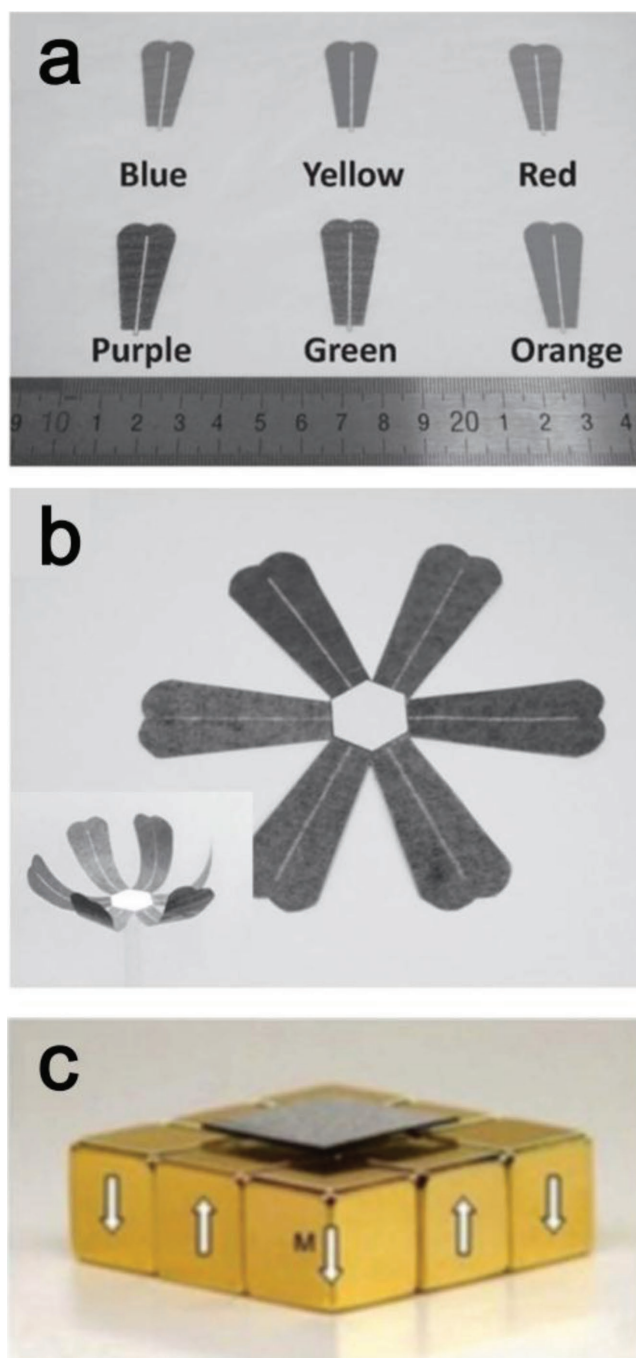


Figure 5. Illustration of graphite used for actuator design. a) Photograph of colorful flower petals made by colored pencils. b) Photograph of an assembled colorful flower actuator. The inset is a picture captured during folding actuation. Reproduced with permission.^[110] Copyright 2016, Wiley-VCH. c) Picture of the PG levitated above the magnet array. Reproduced with permission.^[183] Copyright 2017, Elsevier.

Moreover, PG can float above a strong magnetic field, forming the rarely seen phenomenon: maglev (magnetic levitation) (Figure 5c).^[112,113,183] PG is the greatest diamagnetic material at room temperature ($\chi = -4.5 \times 10^{-4}$).^[112] Photothermal actuators that make use of the maglev characteristic are introduced in Section 3.5.

Amorphous carbon is a type of carbon that does not have any crystalline structure and contains a random distribution of sp^2 , sp^3 , and dangling bonds, so it is considered a completely isotropic material.^[114,115] Unlike anisotropic carbon materials such as CNTs, graphene, or graphite, the thermal conductivity of amorphous carbon in all directions is approximately the same.^[202] The addition of amorphous carbon into other materials endows the material with a uniform photothermal conversion efficiency ($92 \pm 3\%$) and improved light absorption properties. Maggi et al. deposited amorphous carbon film onto SU-8 by sputter deposition to produce a carbon-coated micro-gear actuator.^[116,117] The microgears rotated at different speeds under the same light illumination power as a function of the different carbon thicknesses. This phenomenon was attributed to the different photothermal conversion coefficients of the amorphous carbon coatings.

3. Photothermal Schemes for Light-to-Work Conversion

The actuation process generally depends on the energy density, actuator dimension, and energy conversion efficiency. In addition to active photothermal materials that can convert photon energy to heat effectively, strategies that enable subsequent heat-to-work conversion are of critical importance in developing photothermal actuators. Photothermal schemes for light-to-work conversion determine the energy conversion efficiency and influence the performance of the resultant actuators. Various photothermal schemes such as photothermal-induced expansion/contraction, photothermal phase change, Marangoni effect, and magnetic levitation have been developed for effective actuation. Based on these light-to-work conversion schemes, advanced carbon materials with excellent photothermal conversion efficiency have been coupled with other functional materials to form sophisticated carbon-based photothermal actuators. Photothermal energy conversion mechanisms and relative photothermal actuators are summarized in this section.

3.1. Photothermal Expansion

Thermal expansion is a common phenomenon in which materials change their shape and volume when the surrounding temperature increases because of the increase of the molecular kinetic energy. The CTE, an intrinsic property of materials, has been used to quantify the degree of thermal expansion. The CTEs of typical materials that have been applied to photothermal expansion actuators are listed in **Table 2**. Notably, CNTs and graphene materials have relatively small or even negative CTEs^[118,119]; thus, they may contract with increases in temperature. When materials with large CTEs are combined with photothermal carbon materials that possess small or negative CTEs, the photothermal expansion effect can be utilized for actuator design.^[203,204] A solo material always exhibits isotropic variation in volume upon temperature change. However, in an asymmetric materials system, photothermal effect-induced temperature change forces a mismatch at the bimaterial interface due to the distinct volume change, leading to predictable deforma-

Table 2. CTEs of typical materials for preparing carbon-based actuators.

Material	CTE [ppm K ⁻¹]	Ref.
SWCNT	-1.5	[119,203]
SWCNT (diameter 0.7–1.4 nm)	3–4	[77,170,204]
Graphene	-8.0 ± 0.7	[118]
GO	0.85	[131]
RGO-TEM-PDMS	2000	[123]
PVDF	127	[203]
BOPP	37	[110,131]
Cu	16.9	[121]
Cu ₂ O	5.2	[121]
PC	65–79	[77,204]
PDMS	300	[76]
Paper	10	[110]

tion. To design an actuator, it is essential to form inhomogeneous structures by introducing an anisotropic composition, material property gradient,^[120] or structure gradient.^[6] A metallic actuator constructed of asymmetric bilayer was prepared by Meng et al.^[121] The slightly acidified GO gel was cast on a copper foil and a redox reaction occurred at the interface of GO and Cu, resulting in the formation of a Cu₂O-RGO bilayer structure. The resultant actuator exhibited a rapid response (≈ 2 s) and large deflection curvature (2.4 cm^{-1}) upon light irradiation (**Figure 6a**). This bilayer structure also proves to be sustainable after 50 000 operation cycles.

Compared to inorganic materials, polymers possess much higher CTEs and can expand more obviously upon heating to the same temperature. Hence, the carbon/polymer bilayer systems have become more popular for photothermal actuators.^[77,122] The embedded carbon materials can serve as an efficient light-harvesting and heat-conduction layer, converting photon energy into heat and increasing the local temperature. Because the carbon and polymer materials possess distinct CTEs, asymmetric expansion can lead to an intense mismatch at the material interface, which rolls up the actuators. To amplify the bending degree and promote the mechanical strength, Tang et al. incorporated thermally expanding microspheres (TEMs) with RGO to construct an RGO-TEM-PDMS/PDMS bilayer actuator.^[123] Upon exposure to infrared light, the RGO composite layer absorbed the light and generated heat, inducing an obvious temperature rise. The TEMs with large volume expansion ($\approx 4000\%$) expand as a function of the temperature increase.^[124] The two layers sustain great shear stresses because of the different expansion degree and bent toward the PDMS layer (**Figure 6b**). The incorporation of RGO and TEMs in the PDMS forms an outstanding candidate for light-driven actuators. In this work, the RGO functionalized as energy transfer units and TEMs functioned as excellent mechanical deformation units. Research showed that the Young's modulus of RGO-TEM-PDMS films was increased by 470% from 1.82 to 8.61 MPa after expansion. Therefore, this actuation procedure was irreversible, causing permanent deformation with no need for continuous energy supply. This proposed bilayer structures were used as active hinges for constructing various 3D

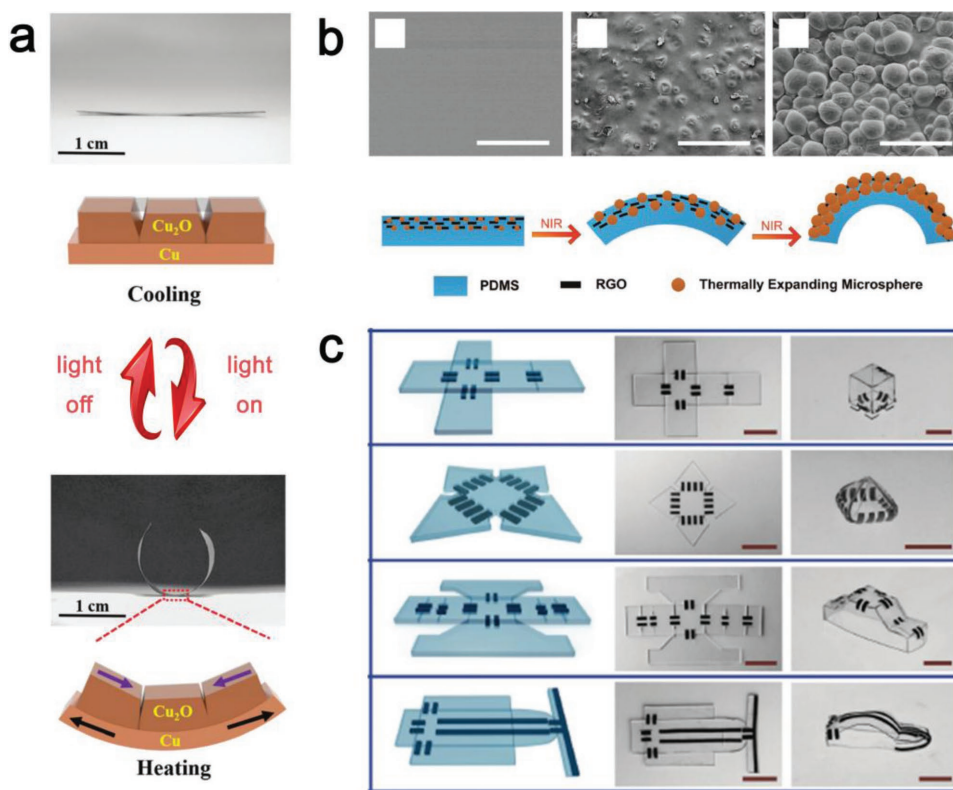


Figure 6. Typical actuators based on photothermal expansion. a) Photographs and illustration of the actuation performed by a Cu₂O–RGO/Cu bilayer. Reproduced with permission.^[121] Copyright 2017, the Royal Society of Chemistry. b) SEM images and schematic illustration of an RGO–TEM–PDMS actuator upon light irradiation. c) Demonstration of light-triggered sophisticated 3D geometries assisted by RGO–TEM–PDMS actuators. Reproduced with permission.^[123] Copyright 2017, Wiley-VCH.

structures (Figure 6c). The bending angle and direction of the hinge can be controlled by tuning the size of the active hinge. Photothermal effects induced expansion and contraction is a common phenomenon that can be observed from a wide range of materials. Thus, the design principle for this kind of actuator is suitable for various carbon embedded bilayer materials.

3.2. Photothermal Desorption

In addition to thermal expansion, reversible adsorption and desorption of guest molecules can also cause the volume change of materials,^[125–128] which provides another opportunity for designing actuators. For example, materials with abundant hydrophilic groups can adsorb water molecules significantly when exposed to moisture, resulting in a distinct increase in volume. Because the temperature increase can cause rapid desorption of the adsorbed water molecules, the volume of the hydrophilic layer usually shows a strong dependence on temperature. According to this basic principle, photothermal actuators have been developed by combining hydrophilic water-adsorption materials with photothermal active carbon materials. Sun and co-workers successfully converted the humidity-responsive actuators into NIR light-driven actuators.^[129] The actuator was constructed using a hydrophilic polydopamine (PDA)-modified RGO and Norland Optical Adhesive (NOA)-63 bilayer structure. The intrinsic NIR absorbance of RGO sheets can be

converted into NIR light into thermal energy to induce the desorption of water molecules in the PDA–RGO layer. Notably, the PDA–RGO layer showed a severe expansion/contraction after water adsorption/desorption, where the NOA-63 remained unchanged all the time. Light irradiation can promote water desorption in the PDA–RGO layer leading to fast bending performance. As compared with humidity actuation that response to adsorption/desorption of water molecules, NIR light actuation can accelerate the desorption rate and thus achieve much shorter response time.

By taking advantage of the water adsorption properties of PDA and GO,^[130] Mu et al. demonstrated an actuator based on PDA–GO and RGO bilayer paper. Using programmed patterns, the actuator can perform more sophisticated motions.^[102] In this work, much faster response was achieved because the presence of GO can promote the adsorption and desorption processes because of its strong interaction with water molecules and photothermal effects, respectively. As the temperature was increased, PDA–GO layer contracted as a result of desorbing water and the hydrophobic RGO was inert to humidity and remained unchanged in volume (Figure 7a). Due to the excellent photothermal effect of RGO and GO and their high flexibility, the actuator was sensitive to light irradiation (a strip with size of 10 mm × 8 mm bent 60° within 2 s). A smart self-folding box was demonstrated. The water adsorption-induced volume swelling in the GO layer has been attributed to the interlayer spacing change, as confirmed by X-ray diffraction

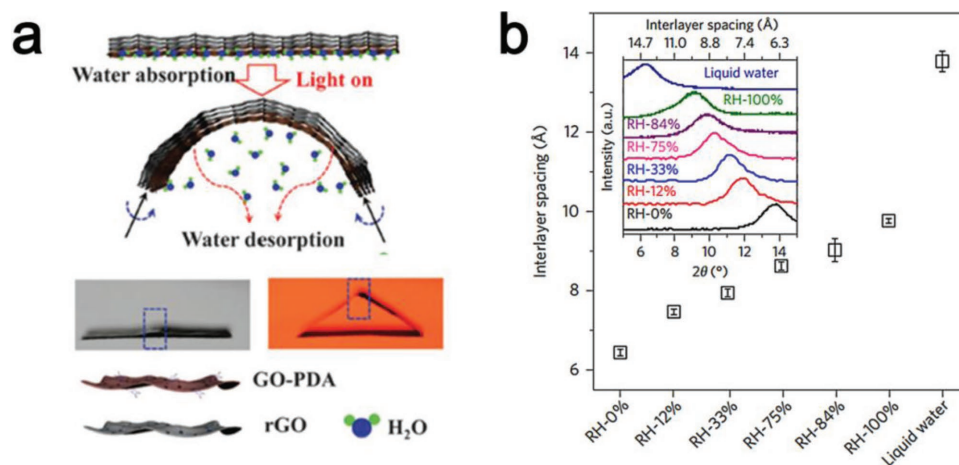


Figure 7. Photothermal desorption strategy for actuator design. a) Schematic illustration of the GO–PDA/RGO bilayer structure and photothermal desorption mechanism. Reproduced with permission.^[102] Copyright 2015, American Association for the Advancement of Science. b) Relationship between the interlayer spacing of graphene and the relative humidity (black line). The moisture content varies as a function of RH. Reproduced with permission.^[132] Copyright 2017, Springer Nature.

patterns (Figure 7b).^[131,132] To increase the deformation degree of the actuators, efforts have been devoted to the increment of the water absorption capability of the hydrophilic materials, such as GO, by introducing more hydrophilic groups or generating higher specific surface area.^[133] In these researches, GO was used as a bifunctional material as it is hydrophilic and photothermally active, revealing great potential for developing photothermal actuators. Notably, GO may suffer from serious problems for practical usage. GO is not stable at high temperature or under light irradiation. The thermal or optical reduction of GO may induce the removal of the hydrophilic oxygen groups and alter the water adsorption capability, making the resultant actuator unstable for long-term usage. Nevertheless, actuation based on photothermal desorption appears to be superior to chemical actuation because it does not need frequent alteration of external chemical environment and can achieve rapid deformation in a noncontact manner.^[103]

3.3. Photothermal Phase Change

Generally, materials have specific properties under a certain condition. With the variation of environmental conditions such as temperature and pressure, some physical properties may change discontinuously, abruptly or significantly, which leads to natural transitions such as the liquid–solid transition, glass transition, and coil–globule transition. These interesting phase-change processes can store and release large amounts of energy that can be utilized for actuating devices.

3.3.1. Hydrophilicity–Hydrophobicity Transition

The phase transition of polymer chains between hydrophilicity and hydrophobicity (phase transform from miscible solvent behavior to a poor solvent behavior state) can be used for photothermal actuation. Typically, at lower temperature, the water molecules reorient around the polymer to decrease the

entropy, resulting in water adsorption and dissolution in water. At higher temperature, the negative entropy predominates the solution system, leading to a phase separation of polymer and water. Such a thermal effect–induced phase transition can cause significant volume change, making photothermal actuation feasible. However, this type of actuator must be used in a liquid environment.

PNIPAAm is an extensively studied material with a reversible hydrophilicity–hydrophobicity transition property at its lower critical solution temperature (LCST, ≈ 32 °C).^[134,135] Upon heating above the LCST, PNIPAAm transform from a swollen state to a shrunken state (Figure 8a), with a volume variation of $\approx 90\%$.^[181] Because of the low thermal conductivity of polymers, macroscopic photothermal actuators based on PNIPAAm usually exhibit an insensitive response, which limits their applications. To overcome this problem, the PNIPAAm has been doped with carbon materials, which promotes the light-to-heat conversion and heat conduction significantly.^[136,137] Javey et al. fabricated photothermal actuators by combining PNIPAAm and SWCNTs to improve the response time up to 5 times faster than those without SWCNTs (Figure 8b).^[137] The ultrafast NIR response was enabled by the synergistic effect of good thermal conductivity and water transportation through the nanotube channels within the gel matrix. The addition of SWCNTs does not significantly affect the LCST of composite materials (Figure 8c). In addition to SWCNTs, GO and RGO have been incorporated with PNIPAAm in photothermal actuators, which demonstrated improved performance.^[138–140,206] In novel research, Gu et al. combined RGO–PNIPAAm fiber with structural color patterns to endow the device with light-controlled reversible bending behavior and tunable color indication (Figure 8d).^[141] The width, spacing, and color can be precisely tailored by adjusting the structural color parameters.^[142] When NIR light was irradiated from one side of the fiber, the expulsion of water molecules on the phototropic side and the shady side underwent different shrinkage extents. The shrinkage drove the two neighboring pores of the striped nanostructures closer, resulting in a blueshift of the structural colors. This

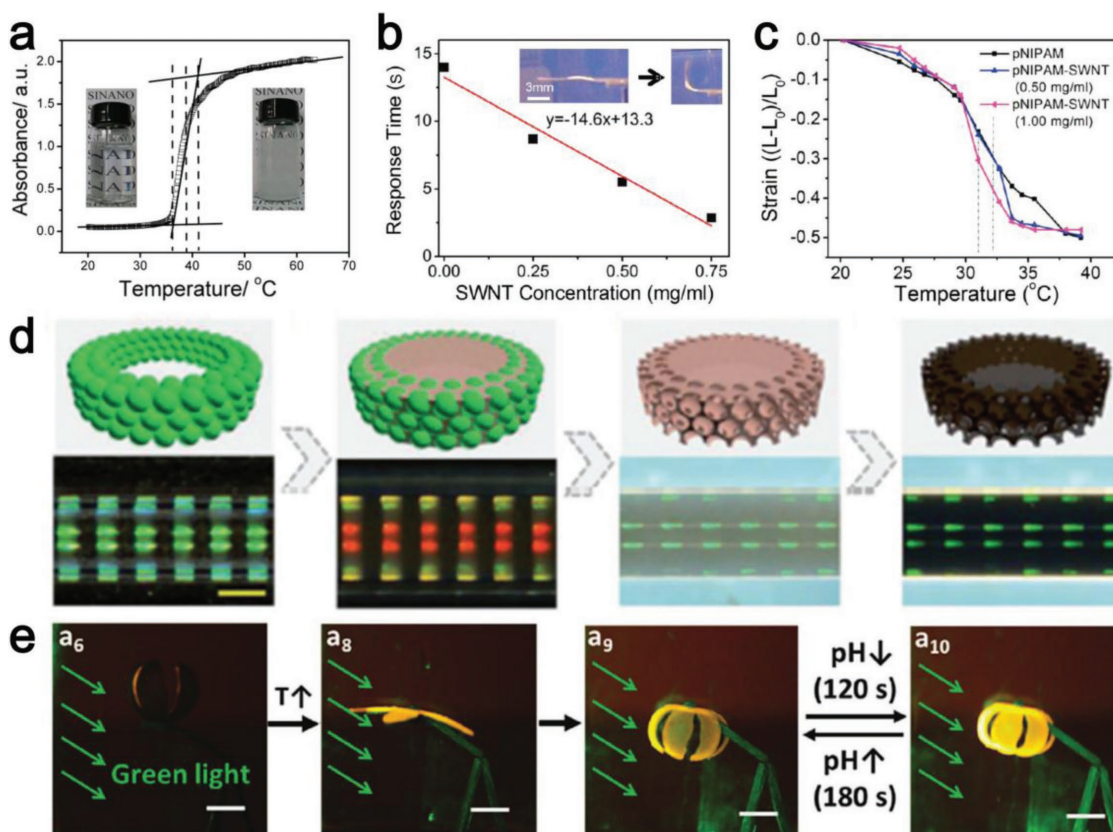


Figure 8. Illustration of photothermal effect-induced hydrophilicity-hydrophobicity transition. a) UV-vis absorption properties of PNIPAAm-based solution changes with the temperature variation. The insets are photographs of the solution at temperatures below and above LCST. Reproduced with permission.^[181] Copyright 2015, American Chemical Society. b) Relationship between the response time and SWCNT concentration of SWCNT-PNIPAAm actuators. c) LCST measurement of actuators with different SWCNT concentrations. Reproduced with permission.^[137] Copyright 2011, American Chemical Society. d) Schematic of PNIPAAm-RGO fibers with inverse opal nanostructures, forming structural color stripes. Reproduced with permission.^[141] Copyright 2017, Wiley-VCH. e) Demonstration of a flower-like GO-PNIPAAm actuator and the fluorescent color display under pH change. Reproduced with permission.^[138] Copyright 2017, Wiley-VCH.

phenomenon can be used as an NIR-light-triggered dynamic barcode labels for anti-counterfeiting of various products. Chen et al. integrated GO-PNIPAAm composite materials with perylene bisimide functionalized hyperbranched polyethylenimine, which has a pH-responsive property. The 3D flower-like actuator could “bloom” when the temperature was increased and the fluorescence intensity was tuned by switching the pH (Figure 8e). These multifunctional actuators are expected to have great potential in neo-concept smart materials.

Because PNIPAAm has a fixed LCST, the hydrophilic to hydrophobic transition is usually confined to a specific temperature range. To broaden the applicable conditions of this type of actuator, elastin-like polypeptides (ELPs) with a repeated monomeric unit (val-pro-gly-X-gly)_n and tunable LCST have been employed for actuators. Because the transition temperature greatly depends on the structural information of the potentially charged “X” residue, ELPs are employed with a programmed transition temperature. ELPs exhibit excellent biocompatibility and can undergo elastic deformations with little loss of energy. Lee and co-workers created ELP-RGO composite actuators showing reversible aggregation and dispersion upon irradiation with an NIR laser at the LCST.^[100] This demonstrated successful coupling of the photothermal response of RGO and the

hydrophilic to hydrophobic transition feature of ELPs and introduced anisotropic porosity to the structure so that the porous region could absorb more than four times more water than the nonporous region and showed more quick diffusion. The actuator bent toward the porous surface, regardless of which side of the material the light was irradiated on. Because the RGO nanosheets were homodispersed into the anisotropically porous ELP hydrogel, these photothermal actuators showed rapid, reversible, and tunable bending motions at certain positions.

3.3.2. Shape Memory Effect

SMPs that possess shape memory properties have been widely used in actuators.^[5,207–209] Generally, SMP-based actuators can be manipulated into a temporary 3D shape, which can return to its permanent shape upon exposure to an external stimulus, such as heat,^[143] light,^[130,144,145] electricity, or solvent.^[146] The controllable shape-changing capability can be attributed to the molecular network that contains more than two separate phases at the solid state. SMPs are fabricated at a higher processing temperature ($T > T_g$), which is responsible for creating the physical crosslinks for the permanent shape. The temporary

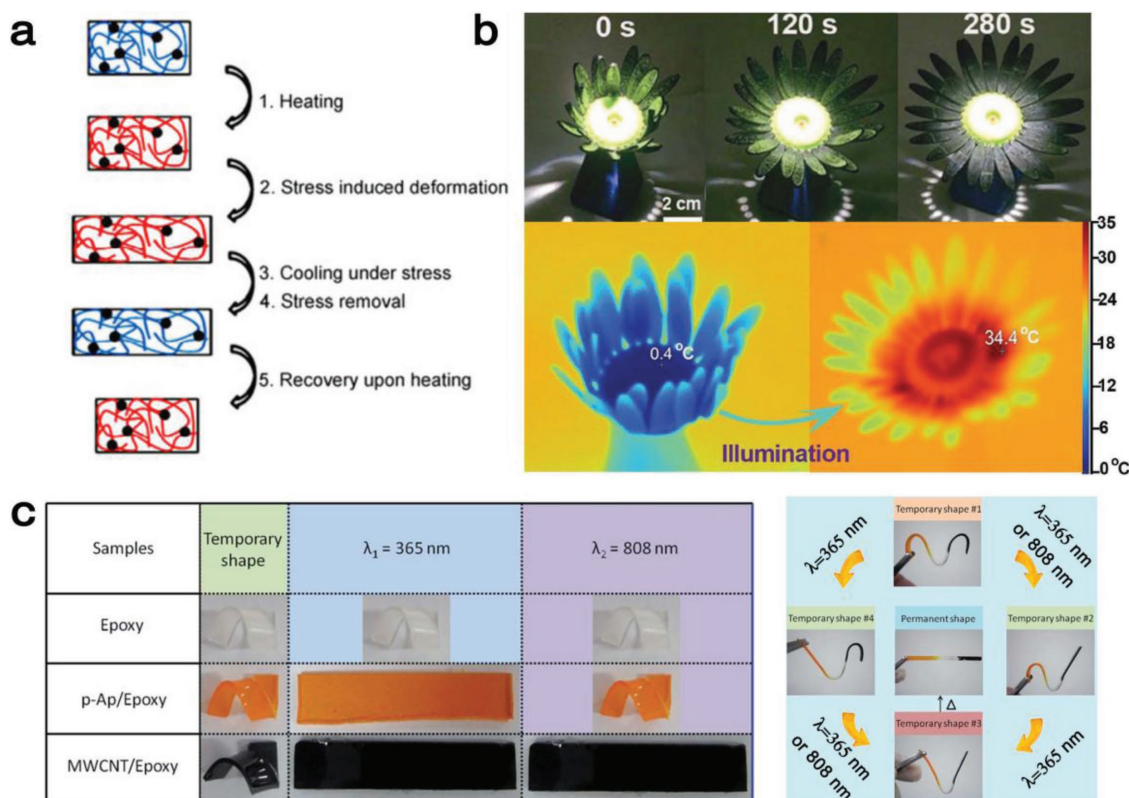


Figure 9. Schematic and typical examples of SMP actuators. a) Conceptual schematic of the shape memory effect. Reproduced with permission.^[91] Copyright 2014, Science China Press. b) Sunflower-like SMP that was fabricated by 3D printing and actuated under 87 mW cm^{-2} (upper images) and infrared images before and after illumination (lower images). Reproduced with permission.^[148] Copyright 2017, Wiley-VCH. c) Multishape memory effect through wavelength-sensitive photomanipulation. Reproduced with permission.^[149] Copyright 2015, the Royal Society of Chemistry.

shape is programmed at a temperature higher than the transition temperature ($T_p > T > T_{\text{tran}}$) and preserved, becoming rigid after cooling ($T < T_{\text{tran}}$) under constant stress (Figure 9a). Any deformation programmed using an external force can be fixed at temperatures less than T_{tran} .^[147] When the temperature is increased above T_{tran} again, the SMPs convert from the rigid state to a soft and pliant state, resulting in shape recovery to the permanent state. SMPs are preferred because of their superior mechanical properties such as low cost, light weight, ease of processing, and potential biocompatibility.

SMPs also suffer from serious problems that restrict their applications in actuating devices. Because polymers usually have poor thermal conductivity, the transition procedures of SMPs are very slow. To address this issue, carbon-based nanomaterials have been successfully added as filler materials to improve the response time of SMPs actuators. The addition of carbon endows the actuators with a light-actuating capability.^[97] Chen et al. fabricated a light-driven polyurethane (PU) SMP actuators by 3D printing using a fused deposition modeling printing method, which avoids structural transitions during the photopolymerization printing process.^[148] The introduction of CB increased the photothermal conversion efficiency but decreased the T_{tran} of the composite materials. Compared with traditional SMPs with planar or tubular structures, 3D printing technology provides an opportunity to fabricate sophisticated 3D shapes at the macrolevel. A cubic frame was demonstrated,

which was predeformed in the squashed temporary state. Upon 160 s of sunlight irradiation, the frame recovered to its permanent state (cubic frame). A more complicated shape memory sunflower was also fabricated (Figure 9b), in which the petals were printed using PU–CB composite materials. Regardless of the shape the petals of the flower were preset into at temperatures greater than T_{tran} , it returned to its original state upon light illumination (87 mW cm^{-2}).

In SMP-based photothermal actuators, light irradiation provides an opportunity for SMPs to release the mechanical energy stored in the temporary state rather than direct transduction of optical energy to mechanical work. SMPs usually have a high capacity for elastic deformation (more than 800%) and considerable output power. When two or more types of materials with varied T_{tran} are integrated, SMPs enable more complicated performance. Research results indicate that light-triggered actuation has great potential to increase the number of temporary shapes of SMP-based actuators. Yu et al. utilized three types of SMP segments (solo epoxy, the *p*-aminodiphenylimide (*p*-Ap)/epoxy, and MWCNT/epoxy composite materials) to realize a multishape memory effect (mSME) upon irradiation of different wavelengths of light (Figure 9c).^[149] The temporary shape was formed at an elevated temperature ($75 \text{ }^\circ\text{C}$), and it maintained this shape until cooling to the room temperature. A photothermal induced shape memory effect (SME) was created by exposing the samples to UV ($\lambda_1 = 365 \text{ nm}$) and NIR

light ($\lambda_2 = 808$ nm). The neat epoxy segment exhibited no temperature increase upon irradiation and thus the shape remained unchanged. The *p*-Ap/epoxy composite showed an increased temperature over T_{tran} only under UV light exposure whereas the MWCNT/epoxy was responsive at both λ_1 and λ_2 . When these three types of SMPs were integrated together and functionalized, it showed three or more temporary shapes when alternately triggered by light sources λ_1 and λ_2 . The remote manipulation of the multishape memory effect makes the shape recovery more flexible.

To increase the number of memory shapes, porous structures are utilized to reduce heat conduction. Light-absorbing materials can convert light energy into heat but the as-generated heat is restrained within the irradiated region because of the mass phonon scattering in porous structures. The insufficient thermal conductivity is essential for selective release of prestrain in temporary shapes, even at the microscale. Chen et al. created multishape memory actuators that could selectively release mechanical energy and generate a variety of temporary shapes.

3.3.3. Nematic–isotropic Transition

Liquid crystals (LCs) are materials that can flow like liquids but their mesogenic units are oriented in a crystal manner.^[150,151] Polymeric liquid crystal materials can be classified into different categories such as thermotropic LCs, lyotropic LCs, metalotropic LCs, and phototropic LCs. Reviews with detailed introductions of their variety have been published.^[152–154] Herein, we focus on thermotropic LCs, as they exhibit variable phases upon temperature change,^[155] which is important for photothermal actuators. The nematic phase is a common state of LCs at room temperature. In this phase, the rod-like units align in a directional order parallel with their long axes. When the temperature increases, the LC transforms into a conventional isotropic liquid phase because the thermal motion can disturb the ordered arrangement.^[156] This transformation of LC units can lead to a volume contraction. Because the LCs demonstrate several fascinating features such topological constraint because of the cross-links,^[157] the oriented order presented by the mesogenic units, and the shape responsiveness due to the strong coupling between the orientation and the mechanical strain, they have been considered good candidates for photothermal actuators.^[158,159] Unlike SMPs, LCEs based on the N-I phase transition can reversibly change their shapes under external stimuli without the need for external mechanical shaping.^[98] Taking advantage of the N-I transition that occurs upon light irradiation, a reversible and dramatic linear contraction (30–400%) has been realized. Kohlmeyer and Chen reported a bilayer actuator consisting of an active layer of SWCNT–LCE composite and an inert layer of silicone.^[160] Upon NIR irradiation, the temperature of SWCNT–LCE can increase to greater than 80 °C within a few seconds, which is higher than the phase transition temperature (64.6 °C). The resultant actuator enables fast and reversible bending with a high light-to-work conversion efficiency. Undoubtedly, incorporation of CNTs into LCEs can make the LCE-based actuators light responsive. However, the poor dispersion of CNTs in LCEs host has been considered a main barrier. Terentjev and co-workers solved this problem

by introducing pyrene into the composites.^[161–163] The presence of pyrene moieties can greatly improve the compatibility of LCEs and CNTs through π – π stacking, leading to remarkable photomechanical property. Meanwhile, the LCE can assist the CNT alignment under mechanical stretching, achieving good thermal conductivity along the CNT orientation. They further applied CNT–LCE into tactile devices producing localized light-to-work actuation.^[164,165,210]

In developing 3D actuators, great efforts have been made to realize 3D reformation of LCEs. LCEs with exchangeable links (xLCEs), a type of vitrimer, have shown the potential to reach this goal. Ji and co-workers realized dynamic 3D structures that can be made and remade into different geometries while repairing mechanical damage and restoring after distortion (**Figure 10**).^[166] These authors proposed a light-sensitive actuator composed of CNTs and xLCEs composite materials, which was employed to realize dynamic 3D structures, such as fabricate, repair, assemble, or heal actuations. Without direct heating, light irradiation can rebuild the alignment of CNT–xLCE units, revealing great potential for spatial control of the orientation arrangement of the materials. The CNTs in the actuator account for the rapid exchange reaction in xLCEs. The as-prepared actuators could reversibly change their length as a result of alternation between nematic and isotropic phases (the temperature was varied between room temperature and 120 °C). Because the numerous directional arrangements can be programmed in one film, the CNT–xLCE materials provide an opportunity to realize dynamic 3D structures on the same sample with great versatility. Additional research confirmed that the N-I transition of CNT–xLCEs can functionalize in the same manner as the shape memory effect. If the samples were deformed below 120 °C, the alignment information remained. The structure could be recovered to the permanent shape by reheating. However, when the actuation was performed at a higher temperature (above 180 °C), all the prewritten alignment information was lost. Therefore, the alignment information can be partially or completely erased by light-to-heat conversion scheme. The photothermal actuations can be conducted at a broad temperature range, which is a benefit of the excellent photothermal properties of CNTs. In this work, a six-petal “flower” could realize more than 20 different shapes (Figure 10d), showing great flexibility in actuation performance.

It is worthy pointing out that the LC-based photoactuators are not only based on obvious order–disorder transitions. Some of them function on only relatively minor changes of LC direction (order–order change).^[167,168] LC order–order change can be further classified by the orientation direction, such as homeotropic alignment (perpendicular to the substrate), homogeneous alignment (parallel to the substrate) and tilt alignment (tilt with respect to the substrate surface normal).^[152] The order–order change of LC units could be realized through photopolarization or photochemical mechanism, and is widely used in LC-based actuators and displays.^[169]

3.3.4. Crystalline Structure Transition

The reversible monoclinic–tetragonal (M–T) transition in VO₂ also enables photothermal actuating because of its structure

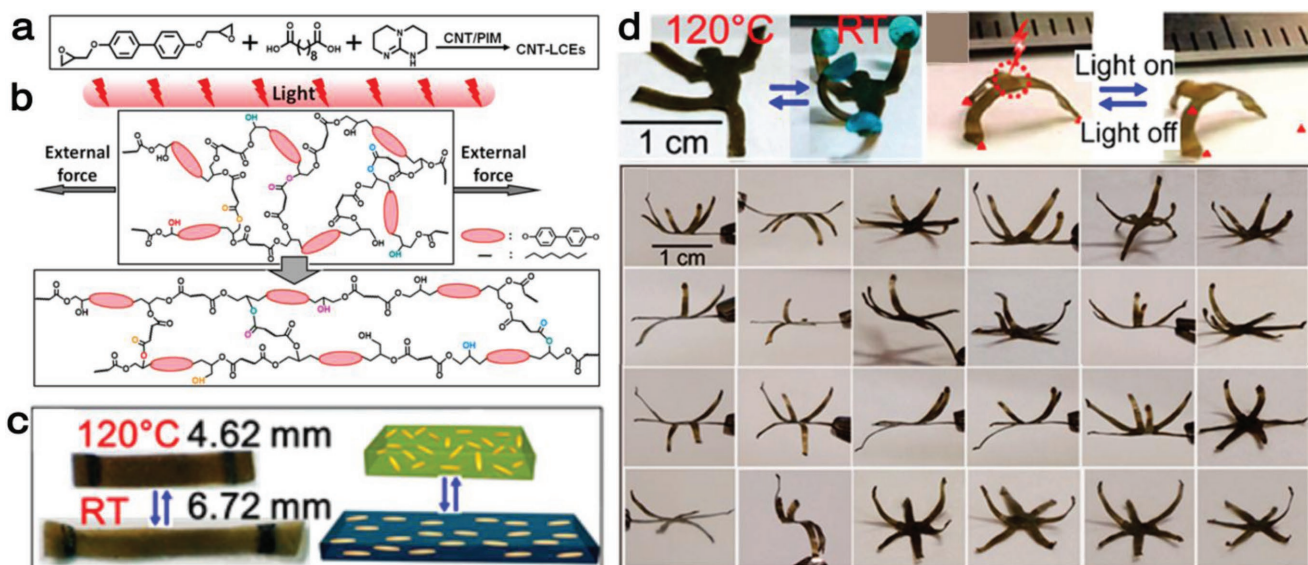


Figure 10. Light-driven CNT-LCE actuator. a) Synthetic method of CNT-LCE material. b) Light-induced alignment of the LC unit. c) Optical images and schematic illustration of the reversible actuation of CNT-xLCE actuators. d) Demonstration of the photothermal performance of actuators made from CNT-xLCE, showing the ability to reconfigure into more than 20 different 3D structures. Reproduced with permission.^[166] Copyright 2016, American Chemical Society.

variation (insulator-metal transition). The M-T phase transition can allow for the miniaturization of high-performance photoactuators (at micro/nanoscale). When the temperature increases to a value greater than the trigger temperature (T_i , ≈ 68 °C), a substantial stress can be generated and converted into mechanical motion (Figure 11a). The response time is on the order of milliseconds. Owing to these merits, VO₂-based actuators have been utilized in MEMS systems. However, unlike carbon materials, VO₂-based actuators usually require higher light intensity to trigger photothermal actuation due to their relative low photothermal conversion efficiency, which more or less hampers their broad application. To address this issue, VO₂ actuators have been integrated with photothermally active CNTs to make use of photenergy. Spulveda and co-workers combined various types of SWCNTs with VO₂ materials to create micromechanical light-driven actuators (Figure 11b).^[170] The actuators showed abrupt bending behavior during the heating-cooling cycle, which indicated that the dominant actuation mechanism was the stress generated during the phase transition of VO₂. The power needed for SWCNT/VO₂ microactuators is only half of that required for VO₂-based actuators (Figure 11c). Recent research reported that the SWCNTs can endow the actuator with a chirality-dependent light response.^[171] Three typical SWCNTs (unsorted, metallic and semiconducting

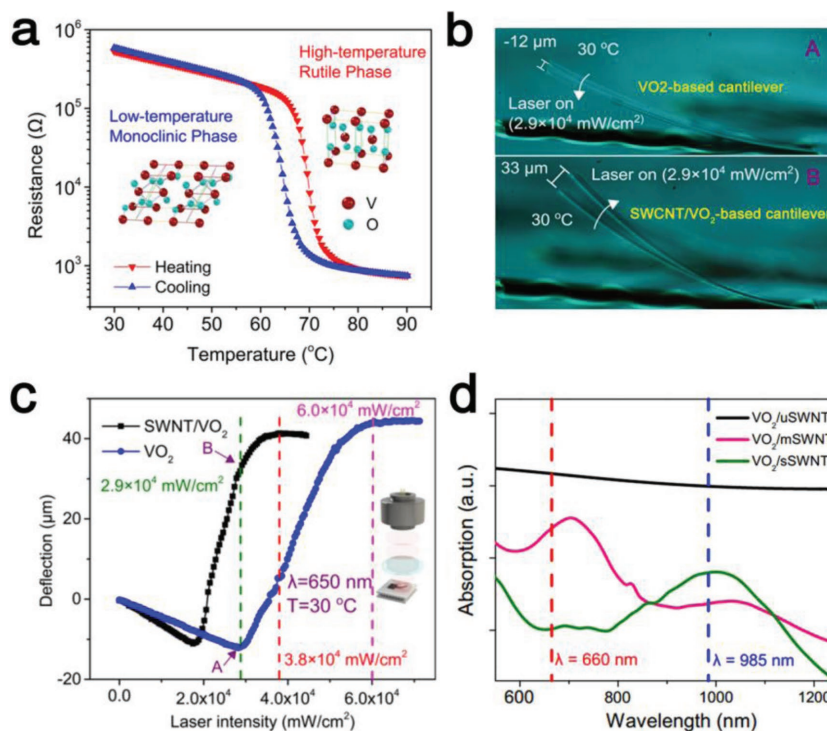


Figure 11. Properties of VO₂-based photothermal actuators. a) Monoclinic-tetragonal character variation as a function of temperature because of the monoclinic to rutile phase change of VO₂. b) The deflection of VO₂ and SWCNT/VO₂ cantilevers as a function of lasers intensity. c) The photographs of VO₂ and SWCNT/VO₂ actuators triggered by 2.9×10^4 mW cm⁻². a-c) reproduced with permission.^[170] Copyright 2015, American Chemical Society. d) Optical absorption spectra of VO₂ actuators combined with unsorted, metallic, and semiconducting SWCNTs. Reproduced with permission.^[171] Copyright 2017, American Association for the Advancement of Science.

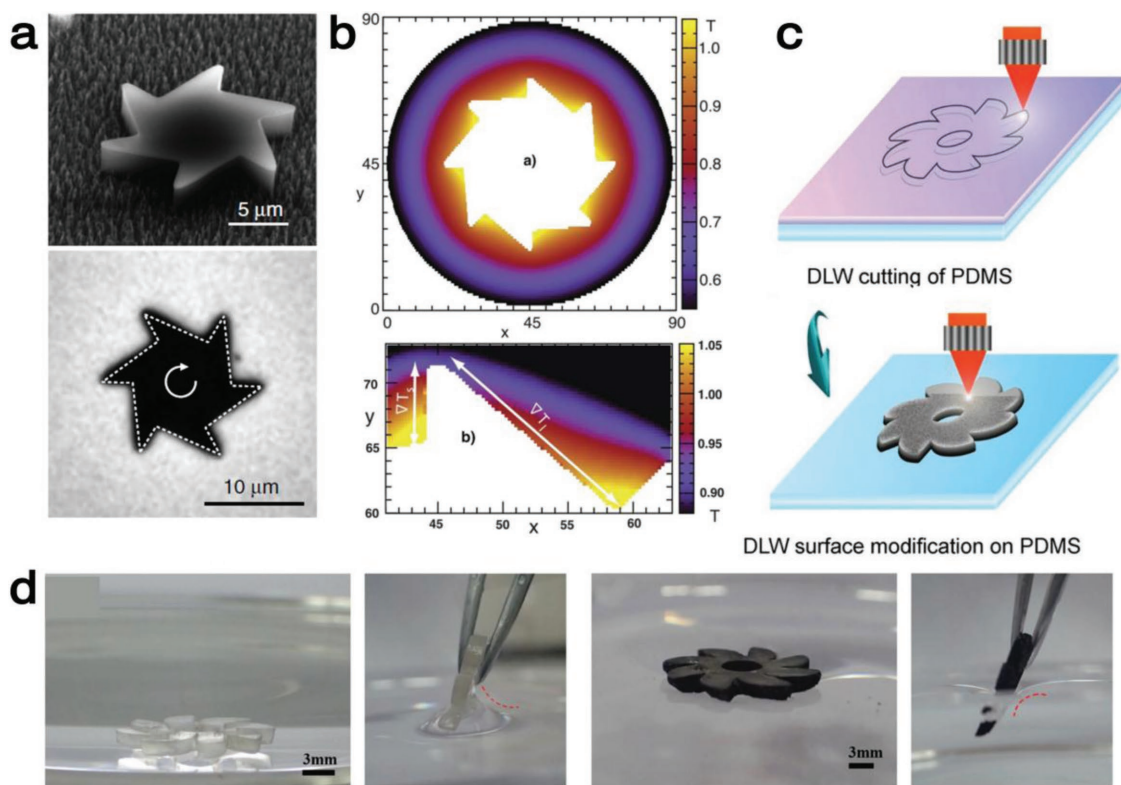


Figure 12. Asymmetric microgears driven by light through the Marangoni effect. a) SEM and microscopy images of a microgear with an outer radius of 8 μm . Reproduced with permission.^[117] Copyright 2015, Nature Publishing Group. b) Simulation of steady-state temperature distribution of the solvent temperature with microgear. Reproduced with permission.^[116] Copyright 2014, the Royal Society of Chemistry. c) Schematic illustration of the facile laser patterning and modifying of the hydrophobic gear. d) Comparison of the wettabilities of pristine and laser-treated PDMS gear. Reproduced with permission.^[173] Copyright 2017, Wiley-VCH.

SWCNTs) were transferred on top of the actuators, and their absorption spectra are shown in Figure 11d. Application of these light-sensitive actuators is expected in MEMS-based logic gates and multiplexers.

3.4. Photothermal Surface Tension Effect

Light-to-work conversion could also be directly realized using the photothermal surface tension effect. A liquid with a high surface tension pulls more strongly on the surrounding liquid than one with a low surface tension (Marangoni effect). Based on this principle, light has been used to generate thermal surface tension gradients at desired positions and cause a floating object to flow away from regions of low surface tension. Generally, when a light beam is directly irradiated onto liquids, surface tension gradients are formed by local photothermal heating. Therefore, a laser or focused sunlight can be used to selectively generate thermal surface tension gradients around a floating object without the need to apply toxic or exhaustible chemical intermediates for actuation.^[172] To increase the output kinetic efficiency, photothermal materials have been integrated with floating devices for light driving via the Marangoni effect. Okawa et al. combined VACNTs with PDMS block and fabricated a light-responsive actuator that can be pulled away on water by light irradiation.^[84] As an outstanding photothermal

material, VACNTs can effectively heat the surrounding liquid under light irradiation. The localized heating can generate a surface tension gradient, leading to linear and rotation motions of the device. The light driving strategy is not limited to a water surface; it is also suitable for various liquids such as glycerol, alcohols, and *N,N*-dimethyl formamide (DMF). To realize rotation motions of devices through the photothermal Marangoni effect, Maggi et al. developed asymmetric microgears on the liquid-air interface that can convert absorbed light into local heat and generate a temperature gradient in the surrounding fluid under wild-field illumination (Figure 12a).^[117] The asymmetric shape breaks the symmetrical stress so that a nonzero total torque is generated because of surface tension gradients. A continuous rotational motion (up to 300 r.p.m.) was realized (Figure 12b). The asymmetric structural design provides a structure-dependent and robust method to produce photothermal actuation.

Despite the abovementioned success, the flexible integration of efficient photothermal materials for such actuators remains challenging. Zhang et al. fabricated a light-driven superhydrophobic floating device with functional surfaces for light absorption and drag reduction.^[173] The direct laser writing technique is employed for arbitrary patterning and surface modification of PDMS elastomers (Figure 12c). A simple laser treatment can carbonize PDMS with a rough surface, leading to a highly efficient photothermal layer with unique superhydrophobicity

(Figure 12d). In this work, a fish, a dozer boat, and rotating gears were fabricated by integrating the carbonized PDMS at the desired position or designing asymmetric structures. The photothermal surface tension effect makes it possible to convert light directly into useful work, which could be used for remote manipulation of devices. However, because the Marangoni effect is generally based on liquid/liquid and liquid/air interface, the surface tension effect manipulation is only workable in the case of objects floating on liquids, which limits its further application.

3.5. Photothermal Actuation under Magnetic Levitation

In addition to the aforementioned photothermal schemes, photothermal actuation can be realized in other ways. For instance, graphite is a typical diamagnetic material that can be levitated in a strong magnetic field at room temperature. In the levitated condition, the diamagnetic material can be effectively manipulated by weak forces without any contact.^[113,174,175] The principle of the actuation is derived from balance of the gravitational levitation and the magnetic force, as described in the Equation (1)

$$mg = F_{\text{meg}} = (\chi V / \mu_0) B dB/dz \quad (1)$$

where m is the mass of PG, g is the acceleration of gravity, χ is the magnetic susceptibility, V is the volume, μ_0 is the permeability of vacuum, B is the magnetic field intensity, and z is the levitation height. Hence, the levitation height and the magnetic susceptibility show an inverse proportion. The static levitation behavior of the PG was investigated by irradiating the graphite with a 405 nm laser (260 mW, Figure 13a). Because the electrons excited by the photothermal effect greatly influence the magnetic susceptibility, light can change the height of PG (Figure 13b). Based on this magnetic levitation effect, Kobayashi and Abe demonstrated a practicable maglev-based actuator system in which the magnetically levitating PG can be driven freely by simple light irradiation.^[175] The PG disk could be driven to any direction based on this photothermal behavior. When the irradiated site was moved from middle to the edge of the disk, the temperature distribution becomes asymmetric.

The magnetic susceptibility is changed at the irradiated site, resulting in variation of the magnetic force. The PG gets off balance and moves toward the same direction the laser is moving (Figure 13c). This work is very important because it is the first maglev-based real-time motion control system. Application of the maglev technique in actuators and manipulators is expected because it can realize frictionless transportation upon simple light driving. However, actuation under magnetic levitation is still at an early stage; it is expected to broaden the practical usage of carbon-based photothermal actuators.

4. Conclusions and Outlook

As a pivotal component enabling direct conversion of various external stimuli into kinetic energy, actuators have been widely used for cutting-edge applications in intelligent systems including MEMS, NEMS, to robots. The unique physical, chemical, and mechanical properties of carbon-based nanomaterials revealed their potential for actuator design. Most carbon materials possess a wideband optical absorption capability that permits absorption of light of various wavelengths and excellent thermal conductivity that enables effective synchronous transfer of heat to other thermally sensitive materials. The photothermal activity makes carbon materials preferred candidates for developing photothermal actuators. In this review, we comprehensively summarized carbon-based photothermal actuators. Several typical carbon materials including graphite, CNTs (e.g., SWCNTs, VACNTs, ACNTs), graphene, graphene derivatives (GO, RGO), and amorphous carbon have been successfully employed for photothermal actuators. Notably, these carbon materials have revealed a series of advantages. For instance, CNTs are widely used in various photothermal actuators because they feature a high length-to-diameter ratio and good flexibility. Moreover, the chiral property of SWCNTs, the anisotropy of ACNTs, and the ultrahigh light absorption capability of VACNTs allow for CNT-based actuators with distinct properties such as chiral deformation, wavelength selectivity, and high energy conversion efficiency. As a new type of 2D carbon nanomaterial with excellent mechanical and electrical properties, graphene has

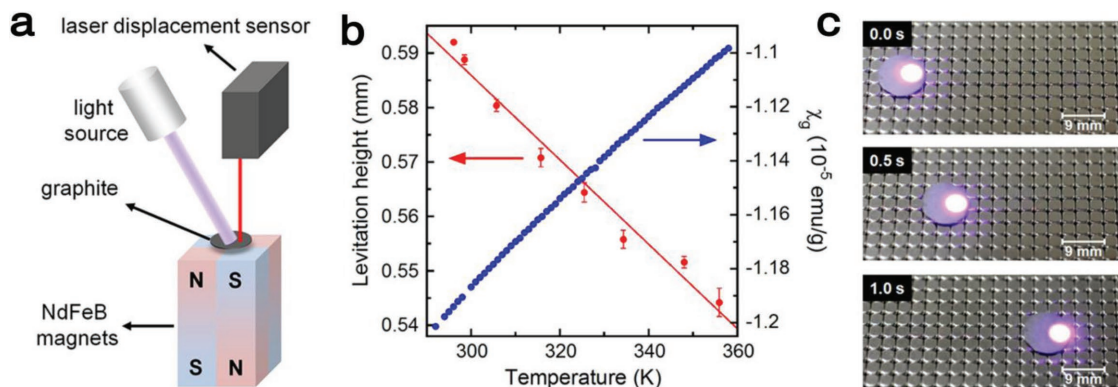


Figure 13. Maglev-based actuator. a) Schematic illustration of experimental measurement of the levitation height influenced by laser irradiation. b) The levitation height and magnetic susceptibility of a PG disk as a function of temperature variation. c) Photographic capture of the directional movement because of magnetic levitation. Reproduced with permission.^[175] Copyright 2012, American Chemical Society.

been adopted in photothermal actuators, in which ultrathin and transparent actuators that can maintain extremely high energy conversion efficiency have been achieved. Graphene derivatives such as GO and RGO are also promising for photothermal actuators. GO can adsorb water molecules and swell itself because of the presence of plenty of oxygen functional groups. Because the adsorption/desorption largely depends on the temperature change, it enables novel photothermal actuation. In addition, graphite, carbon black, and amorphous carbon also contribute to the cost-effective fabrication of high-performance photothermal actuators. Actually, in addition to carbon-based materials, plasmonic particles such as silver nanoparticles, gold nanorods, and gold nanostars can also promote the photothermal conversion efficiency.^[176–178] Due to the surface plasmon resonance, the collective and coherent oscillation of free electrons on nanoparticle surface can lead to effective conversion of photoenergy to heat. As compared with carbon materials, the plasmonic nanoparticles have revealed much higher light-to-heat conversion efficiency and tunable light absorption property. However, the application of these plasmonic nanoparticles in photothermal actuators is somewhat restricted by their high cost, limited heat affected region, and complexity in preparation. Besides, organic dyes have also emerged as photothermal agents since they can convert partial photoenergy into heat in addition to their fluorescence emission.^[179,180] Organic dyes may be biodegradable and biocompatible, which is of benefit to actuator design. However, compared with carbon materials, dyes usually suffer from poor stability under strong irradiation and low light-to-heat conversion efficiency.

Over the past decades, carbon materials have been developed due to their importance in materials science and there are various carbon materials that can easily be prepared or directly purchased to develop photothermal actuators. Carbon materials can act as a functional layer or doping agent for composites to enhance the photothermal activity. Great efforts have been devoted to the preparation and selection of suitable carbon materials for actuator design. Less attention has been paid to the processing of carbon materials. Designable prototyping of carbon materials into desired configurations is also important to fabricate actuators. With solution processing capability, GO appears to be a good choice. The properties of GO can be precisely tuned by selectively removing the oxygen groups and covalently grating other functional groups. Doping of carbon materials with processable polymers, forming a composite, may also benefit actuator fabrication. The current situation can be changed with the rapid progress of advanced processing technologies. With the help of laser processing and 3D printing technologies, carbon-based photothermal actuators can be fabricated in a much easier manner.

In addition to the advanced photothermal materials, photothermal schemes enabling effective light-to-work conversion are also essential for actuator design. Typically, photothermal expansion actuation requires bilayer structures with a large CTE difference between the two layers; photothermal desorption can be applied when the adsorption/desorption of guest molecules can lead to obvious volume changes; specific phase change occurs following the transformation of constituent units as a result of temperature variation; the Marangoni

effect forms a surface tension gradient; and the magnetic susceptibility-guided movement requires a magnetic array. We discussed the principles of different mechanisms and the possibilities for promotion of the response speed, amplitude, and flexibility, respectively. Different photothermal strategies feature distinct merits and also suffer from some limitations at the mean time. Photothermal effects induced expansion and contraction is a common phenomenon that is suitable for developing actuator using various carbon embedded bilayer materials. However, the performance of this kind of actuators might be easily affected by the working temperature. Actuators based photothermal desorption effect can promote the molecules desorption rate and thus shorten the response time significantly. However, the working environment of these actuators is quite limited because it should contain a large amount of active molecules to induce the actuation. Photothermal effect triggered phase change such as wettability changes, shape memory effect, variable phase of thermotropic LCs, and the crystalline structure transition of oxides can store and release large amounts of energy, emerging as an appealing manner to develop photothermal actuators. However, the photothermal-induced phase change is only suitable for special materials. Photothermal surface tension effect enables light-to-work conversion through a novel manner. However, the actuators manipulated via the Marangoni effect are only workable on water surfaces. To comprehensively summarize, the performance of the reported carbon-based photothermal actuators based on different photothermal schemes is shown in **Table 3**. We believe that photothermal actuating strategies are not limited to the examples mentioned above. If the thermal effects can induce significant volume change, detectable deformation, or unbalance of force, direct light-to-work conversion can be realized using photothermal carbon materials.

Despite the rapid advancements in carbon-based photothermal actuators, progress in this field faces several challenges. First, most actuators have been designed and fabricated based on 2D patterns and 3D photothermal actuators are rare. A possible reason to this limitation is the lack of powerful 3D fabrication technologies that enable designable prototyping of multimaterials. Most studies on photothermal actuators are focused on the responsive performance and the pursuit of high speed and large deformation. There is still potential to explore their practical applications in different smart systems and devices. To make individual actuators workable in a holistic device, the flexible integration of such actuators is critical. The third challenge lies in the flexible manipulation of photothermal actuators. The merits of light-driving strategies are not limited to facilitating energy loading and avoiding external connected energy supply systems. Light manipulation can be more flexible because of the multiform tunable parameters. We believe that temporal and spatial control of light sources can be readily realized by tuning their intensity, period, distance, and wavelength of the light sources. With the progress in new types of carbon materials, advanced 3D micro/nanofabrication technologies, novel photothermal schemes, and sophisticated light manipulation strategies, carbon-based photothermal actuators may achieve rapid advancements and find more cutting-edge applications in the near future.

Table 3. Various photothermal actuation strategies and their performance.

Mechanism	Materials	Structure	Size of typical devices	Actuation	Performance (bending angle or curvature)	Light source/ intensity	Response time	Feature	Ref.
Thermal expansion	PC/CNT	Bilayer	25 mm in diameter	Reversible bending	90°	Simulated sunlight 100 mW cm ⁻²	0.87 s	Wavelength-selective	[77,204]
	Cu/Cu ₂ O/RGO	Multilayer	4 cm × 5 mm	Reversible bending	1.3 cm ⁻¹	1000 Infrared light	2 s		[121]
	CNT/PDMS	Bilayer	21 mm × 14 mm	Reversible bending, jumping	215°	Sunlight 250 mW cm ⁻²	0.83 s 7 s recovery		[76]
	RGO-TEM-PDMS/PDMS	Bilayer	20 mm × 2 mm	Permanent bending	180°	IR lamp 250 W	30 s		[123]
	GNP-PDMS/Cr	Bilayer	15 mm × 2.5 mm	Reversible bending	40°	IR 550 mW cm ⁻²	1 s 3 s recovery		[193]
	PDMS-GNP/PDMS	Bilayer	7 mm × 1 mm	Reversible bending	1500 μm	NIR 29.5 W mm ⁻²	3.4 s		[99,205]
	ACNT/paraffin wax	Bilayer	20 mm × 4 mm	Reversible bending or twisting	85°	Visible light 100 mW cm ⁻²	0.87 s 1.86 s		[79]
	RGO-CNT/PDMS	Bilayer	24 mm × 5 mm	bending	479°	Simulated sunlight 250 W cm ⁻²	3.6 s 6.8 s		[122]
Thermal desorption	CNP	Anisotropic film	5 mm × 2 mm	Reversible bending or jumping	≈110°	UV light (365 nm) 200 mW cm ⁻²	0.05 s		[125]
	GO	Asymmetric film	2.5 cm × 0.5 cm	Reversible bending	–	IR light	<1 s		[133]
	RGO/GO	Gradient-reduced GO/RGO	20 mm × 2 mm	Reversible bending	95°	IR light 150 mW cm ⁻²	0.3 s		[182]
	GO-PDA/RGO	Dual gradient structure	10 mm × 8 mm	Reversible bending	60°	NIR light 100 mW cm ⁻²	2 s		[102]
	PDA-RGO/NOA-63	Bilayer	1.2 cm × 0.5 cm	Reversible bending	90°	NIR light 22 mW cm ⁻²	2 s 5 s recovery		[129]
Thermal expansion and desorption	SWCNT/PVDF	Bilayer	2 cm × 2 cm	Reversible bending or twisting	910°	100 W lamp	1.06 s		[203]
	GO/BOPP	Bilayer	15 mm × 2 mm	Reversible bending or twisting	2.8 cm ⁻¹	NIR light 300 mW cm ⁻²	10 s V _m = 0.28 cm ⁻¹ s ⁻¹	Light to heat 76.5%	[131]
	BOPP/graphite/paper	multilayer	30 mm × 10 mm	Reversible bidirectional bending	1.9 cm ⁻¹	NIR light 300 mW cm ⁻²	10 s 15 s recovery	Light to heat 85.5%	[110]
Soluble-insoluble transition	GO-PNIPAAm/PNIPAAm	Bilayer	50 mm × 10 mm	Reversible contraction, bending or twisting	Shift 21 mm (34 mm in length)	IR light 0.8 W cm ⁻²	110 s		[140,206]
	PNIPAAm-RGO	Composite fiber	1.1 mm in diameter	Reversible bending, structure color shift	50°	NIR light	40 s	Asymmetric irradiation	[141]
	PNIPAAm-RGO/PAAm	Bilayer	215 μm × 760 μm	Reversible bending	360°	Blue light or sunlight 41.8 mW cm ⁻²	30 s		[139]

Table 3. Continued.

Mechanism	Materials	Structure	Size of typical devices	Actuation	Performance (bending angle or curvature)	Light source/ intensity	Response time	Feature	Ref.
	SWCNT–PNIPAAm–AuNRs	Composite membrane	2.54 cm ²	Tunable pore size	35 890 m ² h ⁻¹ bar ⁻¹	NIR laser 3.38 W cm ⁻²	4 s		[181]
	ELP–RGO	Anisotropic film	cm	Reversible bending	75°	NIR laser 5.7 W cm ⁻²	3 s >10 s recovery		[100]
	SWCNT–PNIPAAm/LDPE	Bilayer	50 mm × 5 mm	Reversible bending	90°	NIR laser	2.7 s		[137]
SME	PU–CB	3D structure (through 3D printing)	50 mm × 20 mm	Single-shape memory	140°	Sunlight 198 mW cm ⁻²	180 s	Light to heat ≈10%	[148]
	Epoxy/ <i>p</i> -Ap–epoxy/MWCNT–epoxy	Separated segments	30 mm × 5 mm	Triple/multishape memory	–	λ ₁ = 808 nm 2.8 W cm ⁻² ; λ ₂ = 365 nm 270 mW cm ⁻²	<10 s	Wavelength-selective	[149]
	GO–PVDF–HFP	Composite film	1 mm × 1 mm	Single-shape memory	–	450 nm light 54 mW cm ⁻²	2 s	Tumbler movement	[207]
	CNT–boron nitride–epoxy	Composite film	60 mm × 10 mm	Single-shape memory	180°	NIR light heating oven	60 s		[208]
	TPU–SRGO or TPU–SCNT	Composite film	30 mm × 10 mm	Stress recovery	Elongated by 250%	IR > 900 nm 30 mW cm ⁻²	18 s	Max. weight 107.9 g	[106,209]
Nematic–isotropic transition	CNT–xLCE	Composite film	5 mm	Reshaped or reconfigured	–	808 nm NIR light 0.84 W cm ⁻²	Few seconds	Can be performed at –130 °C	[166]
	SWCNT or IR dye–LCE/silicone	Bilayer	23 mm × 3 mm	Reversible bending	0.28 mm ⁻¹	NIR light 11 mW mm ⁻²	10 s	Wavelength-selective	[160]
	Azo–LCP–CNT	Composite strip	2 cm × 2 mm	Reversible deflection	12 mm	UV light 50–100 mW cm ⁻²	<2 s		[43]
	CNT–LCE	Composite strip	3 mm × 0.8 mm	Reversible bending		Broad-spectrum light 30 mW cm ⁻²	5 s		[165,210]
	GO–LC	Composite strip	20 mm × 5 mm	Reversible bending	–	450 nm UV light 54 mW cm ⁻² 808 nm NIR light 66 mW cm ⁻²	1.5 s		[156]
Monoclinic–tetragonal transition	VO ₂ /SWCNT/SiO ₂	multilayer	400 μm × 40 μm	Reversible deflection	40 μm	660 nm 985 nm laser 80 mW	<5 ms	Wavelength-selective	[170,171]
Marangoni effect	Carbonized PDMS	Microgear	1.5 cm in diameter	Rotation; self-propel	1.57 rad s ⁻¹ 2 cm	Laser or sunlight 0.9 W cm ⁻²	2.4 s	Liquid–air interface	[173]
	Amorphous carbon/SU-8	Microgear	8 μm in diameter	Rotation	300 r.p.m.	Incoherent light	–	Liquid–air interface	[116,117]
	VACNT–PDMS	Bulk object	mm	Linear or rotation motion	8 cm	785 nm laser 450 mW	1 s	Liquid–air interface Output force ≈29 μN	[84]
Magnetic susceptibility change	Pyrolytic graphite	Disk	3 mm in diameter	Rotation or linear motion	200 r.p.m.	405 nm 300 mW	–		[175]

Acknowledgements

The authors would like to acknowledge the support by the National Key Research and Development Program of China and National Natural Science Foundation of China (NSFC) under Grants #2017YFB1104300, #61590930, #61522503, #61775078, and #61605055.

Conflict of Interest

The authors declare no conflict of interest.

Keywords

carbon nanotubes, graphene, light to heat conversion, photothermal actuators, photothermal effects

Received: March 30, 2018

Revised: June 11, 2018

Published online: August 12, 2018

- [1] E. L. Chaikof, *Nature* **2010**, 465, 44.
- [2] W. S. Y. Wong, M. Li, D. R. Nisbet, V. S. J. Craig, Z. Wang, A. Tricoli, *Sci. Adv.* **2016**, 2, e1600417.
- [3] R. Kempaiah, Z. Nie, J. *Mater. Chem. B* **2014**, 2, 2357.
- [4] Y. Liu, B. Shaw, M. D. Dickey, J. Genzer, *Sci. Adv.* **2017**, 3, e1602417.
- [5] B. Q. Chan, Z. W. Low, S. J. Heng, S. Y. Chan, C. Ow, X. J. Loh, *ACS Appl. Mater. Interfaces* **2016**, 8, 10070.
- [6] L. Ionov, *Adv. Funct. Mater.* **2013**, 23, 4555.
- [7] Q. Chen, X. Yu, Z. Pei, Y. Yang, Y. Wei, Y. Ji, *Chem. Sci.* **2017**, 8, 724.
- [8] Y. Park, M. P. Gutierrez, L. P. Lee, *Sci. Rep.* **2016**, 6, 39402.
- [9] Q. Zhao, J. W. Dunlop, X. Qiu, F. Huang, Z. Zhang, J. Heyda, J. Dzubiella, M. Antonietti, J. Yuan, *Nat. Commun.* **2014**, 5, 4293.
- [10] Y.-L. Sun, W.-F. Dong, L.-G. Niu, T. Jiang, D.-X. Liu, L. Zhang, Y.-S. Wang, Q.-D. Chen, D.-P. Kim, H.-B. Sun, *Light: Sci. Appl.* **2014**, 3, e129.
- [11] L. Chen, M. Weng, W. Zhang, Z. Zhou, Y. Zhou, D. Xia, J. Li, Z. Huang, C. Liu, S. Fan, *Nanoscale* **2016**, 8, 6877.
- [12] D. Gao, W. Ding, M. Nieto-Vesperinas, X. Ding, M. Rahman, T. Zhang, C. Lim, C.-W. Qiu, *Light: Sci. Appl.* **2017**, 6, e17039.
- [13] A. H. Gelebart, D. Jan Mulder, M. Varga, A. Konya, G. Vantomme, E. W. Meijer, R. L. B. Selinger, D. J. Broer, *Nature* **2017**, 546, 632.
- [14] Q. Li, C. Liu, Y.-H. Lin, L. Liu, K. Jiang, S. Fan, *ACS Nano* **2015**, 9, 409.
- [15] M. Amjadi, M. Sitti, *ACS Nano* **2016**, 10, 10202.
- [16] S. Fusco, M. S. Sakar, S. Kennedy, C. Peters, R. Bottani, F. Starsich, A. Mao, G. A. Sotiriou, S. Pane, S. E. Pratsinis, D. Mooney, B. J. Nelson, *Adv. Mater.* **2014**, 26, 952.
- [17] W. Hu, G. Z. Lum, M. Mastrangeli, M. Sitti, *Nature* **2018**, 554, 81.
- [18] D.-D. Han, Y.-L. Zhang, Y. Liu, Y.-Q. Liu, H.-B. Jiang, B. Han, X.-Y. Fu, H. Ding, H.-L. Xu, H.-B. Sun, *Adv. Funct. Mater.* **2015**, 25, 4548.
- [19] G. Wang, H. Xia, X.-C. Sun, C. Lv, S.-X. Li, B. Han, Q. Guo, Q. Shi, Y.-S. Wang, H.-B. Sun, *Sens. Actuators, B* **2018**, 255, 1415.
- [20] S. Lu, Y. Liu, N. Shao, B. Panchapakesan, *Nanotechnology* **2007**, 18, 065501.
- [21] X. Zang, Q. Zhou, J. Chang, Y. Liu, L. Lin, *Microelectron. Eng.* **2015**, 132, 192.
- [22] L. Hines, K. Petersen, G. Z. Lum, M. Sitti, *Adv. Mater.* **2017**, 29, 1603483.
- [23] H. Zeng, P. Wasylczyk, D. S. Wiersma, A. Priimagi, *Adv. Mater.* **2017**, 30, 1703554.
- [24] D. Rus, M. T. Tolley, *Nature* **2015**, 521, 467.
- [25] S. Felton, M. Tolley, E. Demaine, D. Rus, R. Wood, *Science* **2014**, 345, 644.
- [26] D. Floreano, R. J. Wood, *Nature* **2015**, 521, 460.
- [27] E. R. Kay, D. A. Leigh, F. Zerbetto, *Angew. Chem., Int. Ed. Engl.* **2007**, 46, 72.
- [28] J. Wang, Z. Xiong, X. Zhan, B. Dai, J. Zheng, J. Liu, J. Tang, *Adv. Mater.* **2017**, 29, 1701451.
- [29] P. Fratzl, F. G. Barth, *Nature* **2009**, 462, 442.
- [30] H. Jia, J. Wang, X. Zhang, Y. Wang, *ACS Macro Lett.* **2013**, 3, 86.
- [31] X. Dou, J. Wang, X. Lu, M. Zhang, Y. Qin, Y. Wang, P. Zhang, Z.-X. Guo, *RSC Adv.* **2016**, 6, 112241.
- [32] S. A. Morin, R. F. Shepherd, S. W. Kwok, A. A. Stokes, A. Nemiroski, G. M. Whitesides, *Science* **2012**, 337, 828.
- [33] H. Yuk, S. Lin, C. Ma, M. Takaffoli, N. X. Fang, X. Zhao, *Nat. Commun.* **2017**, 8, 14230.
- [34] M. J. Villangca, D. Palima, A. R. Bañas, J. Glückstad, *Light: Sci. Appl.* **2016**, 5, e16148.
- [35] H. Zeng, O. M. Wani, P. Wasylczyk, A. Priimagi, *Macromol. Rapid Commun.* **2018**, 39, 1700224.
- [36] A. H. Gelebart, D. J. Mulder, G. Vantomme, A. Schenning, D. J. Broer, *Angew. Chem., Int. Ed. Engl.* **2017**, 56, 13436.
- [37] J. Ni, C. Wang, C. Zhang, Y. Hu, L. Yang, Z. Lao, B. Xu, J. Li, D. Wu, J. Chu, *Light: Sci. Appl.* **2017**, 6, e17011.
- [38] L. Jiang, A.-D. Wang, B. Li, T.-H. Cui, Y.-F. Lu, *Light: Sci. Appl.* **2018**, 7, 17134.
- [39] G. L. Liu, J. Kim, Y. Lu, L. P. Lee, *Nat. Mater.* **2006**, 5, 27.
- [40] D. D. Han, Y. L. Zhang, J. N. Ma, Y. Q. Liu, B. Han, H. B. Sun, *Adv. Mater.* **2016**, 28, 8328.
- [41] C. Zhu, C. Ninh, C. J. Bettinger, *Biomacromolecules* **2014**, 15, 3474.
- [42] H. Lim, T. Park, J. Na, C. Park, B. Kim, E. Kim, *NPG Asia Mater.* **2017**, 9, e399.
- [43] X. Sun, W. Wang, L. Qiu, W. Guo, Y. Yu, H. Peng, *Angew. Chem., Int. Ed. Engl.* **2012**, 51, 8520.
- [44] H. Xin, B. Li, *Light: Sci. Appl.* **2014**, 3, e205.
- [45] Q. Xu, T. Ma, M. Danesh, B. N. Shivananju, S. Gan, J. Song, C.-W. Qiu, H.-M. Cheng, W. Ren, Q. Bao, *Light: Sci. Appl.* **2016**, 6, e16204.
- [46] P. Mestres, J. Berthelot, S. S. Aćimović, R. Quidant, *Light: Sci. Appl.* **2016**, 5, e16092.
- [47] J. Wang, J. Zhao, Y. Li, M. Yang, Y.-Q. Chang, J.-P. Zhang, Z. Sun, Y. Wang, *ACS Macro Lett.* **2015**, 4, 392.
- [48] Y. Jiao, K. Liu, G. Wang, Y. Wang, X. Zhang, *Chem. Sci.* **2015**, 6, 3975.
- [49] Y. Chen, H. Yu, M. Quan, L. Zhang, H. Yang, Y. Lu, *RSC Adv.* **2015**, 5, 4675.
- [50] W. Nakanishi, K. Minami, L. K. Shrestha, Q. Ji, J. P. Hill, K. Ariga, *Nano Today* **2014**, 9, 378.
- [51] A. A. Balandin, *Nat. Mater.* **2011**, 10, 569.
- [52] Z. Liu, X. J. Liang, *Theranostics* **2012**, 2, 235.
- [53] N. V. Medhekar, A. Ramasubramaniam, R. S. Ruoff, V. B. Shenoy, *ACS Nano* **2010**, 4, 2300.
- [54] M. A. Rafiee, J. Rafiee, Z. Wang, H. Song, Z.-Z. Yu, N. Koratkar, *ACS Nano* **2009**, 3, 3884.
- [55] Y. Shen, A. G. Skirtach, T. Seki, S. Yagai, H. Li, H. Moehwald, T. Nakanishi, *J. Am. Chem. Soc.* **2010**, 132, 8566.
- [56] D. K. Lim, A. Barhoumi, R. G. Wylie, G. Reznor, R. S. Langer, D. S. Kohane, *Nano Lett.* **2013**, 13, 4075.
- [57] M. Acik, G. Lee, C. Mattevi, M. Chhowalla, K. Cho, Y. J. Chabal, *Nat. Mater.* **2010**, 9, 840.
- [58] D. Li, D. Han, S.-N. Qu, L. Liu, P.-T. Jing, D. Zhou, W.-Y. Ji, X.-Y. Wang, T.-F. Zhang, D.-Z. Shen, *Light: Sci. Appl.* **2016**, 5, e16120.
- [59] R. Prasher, *Science* **2010**, 328, 185.

- [60] J. H. Seol, I. Jo, A. L. Moore, L. Lindsay, Z. H. Aitken, M. T. Pettes, X. Li, Z. Yao, R. Huang, D. Broido, N. Mingo, R. S. Ruoff, L. Shi, *Science* **2010**, 328, 213.
- [61] S. Malik, F. M. Ruddock, A. H. Dowling, K. Byrne, W. Schmitt, I. Khalakhan, Y. Nemoto, H. Guo, L. K. Shrestha, K. Ariga, J. P. Hill, *Beilstein J. Nanotechnol.* **2018**, 9, 801.
- [62] S. Malik, Y. Nemoto, H. Guo, K. Ariga, J. P. Hill, *Beilstein J. Nanotechnol.* **2016**, 7, 1260.
- [63] L. J. Cote, R. Cruz-Silva, J. Huang, *J. Am. Chem. Soc.* **2009**, 131, 11027.
- [64] C. Lin, Y. Zhu, *Appl. Opt.* **2016**, 55, 2324.
- [65] K. Ariga, K. Minami, L. K. Shrestha, *Analyst* **2016**, 141, 2629.
- [66] L. K. Shrestha, R. G. Shrestha, S. Joshi, R. Rajbhandari, N. Shrestha, M. P. Adhikari, R. R. Pradhananga, K. Ariga, *J. Inorg. Organomet. Polym. Mater.* **2017**, 27, 48.
- [67] J. Na, J. S. Heo, M. Han, H. Lim, H. O. Kim, E. Kim, *Adv. Funct. Mater.* **2017**, 27, 1604260.
- [68] A. M. Marconnet, M. A. Panzer, K. E. Goodson, *Rev. Mod. Phys.* **2013**, 85, 1295.
- [69] G. Fugallo, A. Cepellotti, L. Paulatto, M. Lazzeri, N. Marzari, F. Mauri, *Nano Lett.* **2014**, 14, 6109.
- [70] P. Tao, W. Shang, C. Song, Q. Shen, F. Zhang, Z. Luo, N. Yi, D. Zhang, T. Deng, *Adv. Mater.* **2015**, 27, 428.
- [71] X. Huang, Q. Qian, X. Zhang, W. Du, H. Xu, Y. Wang, *Part. Part. Syst. Character.* **2013**, 30, 235.
- [72] E. T. Thostenson, Z. F. Ren, T. W. Chou, *Compos. Sci. Technol.* **2001**, 61, 1899.
- [73] M. F. L. De Volder, S. H. Tawfik, R. H. Baughman, A. J. Hart, *Science* **2013**, 339, 535.
- [74] H. Koerner, G. Price, N. A. Pearce, M. Alexander, R. A. Vaia, *Nat. Mater.* **2004**, 3, 115.
- [75] M. F. Yu, B. S. Files, S. Arepalli, R. S. Ruoff, *Phys. Rev. Lett.* **2000**, 84, 5552.
- [76] Y. Hu, J. Liu, L. Chang, L. Yang, A. Xu, K. Qi, P. Lu, G. Wu, W. Chen, Y. Wu, *Adv. Funct. Mater.* **2017**, 27, 1704388.
- [77] X. Zhang, Z. Yu, C. Wang, D. Zarrouk, J. W. Seo, J. C. Cheng, A. D. Buchan, K. Takei, Y. Zhao, J. W. Ager, J. Zhang, M. Hettick, M. C. Hersam, A. P. Pisano, R. S. Fearing, A. Javey, *Nat. Commun.* **2014**, 5, 2983.
- [78] K. Okano, I. Noguchi, T. Yamashita, *Macromolecules* **2010**, 43, 5496.
- [79] J. Deng, J. Li, P. Chen, X. Fang, X. Sun, Y. Jiang, W. Weng, B. Wang, H. Peng, *J. Am. Chem. Soc.* **2016**, 138, 225.
- [80] W. Xiong, Y. Liu, L. J. Jiang, Y. S. Zhou, D. W. Li, L. Jiang, J. F. Silvain, Y. F. Lu, *Adv. Mater.* **2016**, 28, 2002.
- [81] Y. Liu, J. Genzer, M. D. Dickey, *Prog. Polym. Sci.* **2016**, 52, 79.
- [82] Z.-P. Yang, L. Ci, J. A. Bur, S.-Y. Lin, P. M. Ajayan, *Nano Lett.* **2008**, 8, 446.
- [83] Q. M. Zou, L. M. Deng, D. W. Li, Y. S. Zhou, H. R. Golgir, K. Keramatnejad, L. S. Fan, L. Jiang, J. F. Silvain, Y. F. Lu, *ACS Appl. Mater. Interfaces* **2017**, 9, 37340.
- [84] D. Okawa, S. J. Pastine, A. Zettl, J. M. J. Frechet, *J. Am. Chem. Soc.* **2009**, 131, 5396.
- [85] S. V. Ahir, E. M. Terentjev, *Phys. Rev. Lett.* **2006**, 96, 133902.
- [86] J. N. Wang, Y. L. Zhang, Y. Liu, W. Zheng, L. P. Lee, H. B. Sun, *Nanoscale* **2015**, 7, 7101.
- [87] C. Wu, J. Feng, L. Peng, Y. Ni, H. Liang, L. He, Y. Xie, *J. Mater. Chem.* **2011**, 21, 18584.
- [88] J. W. Jiang, B. S. Wang, J. S. Wang, H. S. Park, *J. Phys.: Condens. Matter* **2015**, 27, 083001.
- [89] K. S. Novoselov, V. I. Fal'ko, L. Colombo, P. R. Gellert, M. G. Schwab, K. Kim, *Nature* **2012**, 490, 192.
- [90] F. Zhao, Y. Zhao, N. Chen, L. Qu, *Mater. Today* **2016**, 19, 146.
- [91] Y. Wong, J. Kong, L. K. Widjaja, S. S. Venkatraman, *Sci. China: Chem.* **2014**, 57, 476.
- [92] X. Yu, H. Cheng, M. Zhang, Y. Zhao, L. Qu, G. Shi, *Nat. Rev. Mater.* **2017**, 2, 17046.
- [93] G.-K. Lim, Z.-L. Chen, J. Clark, R. G. S. Goh, W.-H. Ng, H.-W. Tan, R. H. Friend, P. K. H. Ho, L.-L. Chua, *Nat. Photonics* **2011**, 5, 554.
- [94] C. Lee, X. Wei, J. W. Kysar, J. Hone, *Science* **2008**, 321, 385.
- [95] A. A. Balandin, S. Ghosh, W. Bao, I. Calizo, D. Teweldebrhan, F. Miao, C. N. Lau, *Nano Lett.* **2008**, 8, 902.
- [96] D. Meng, S. Yang, L. Guo, G. Li, J. Ge, Y. Huang, C. W. Bielawski, J. Geng, *Chem. Commun.* **2014**, 50, 14345.
- [97] D. H. Yi, H. J. Yoo, S. S. Mahapatra, Y. A. Kim, J. W. Cho, *J. Colloid Interface Sci.* **2014**, 432, 128.
- [98] R. S. Kularatne, H. Kim, J. M. Boothby, T. H. Ware, *J. Polym. Sci., Part B: Polym. Phys.* **2017**, 55, 395.
- [99] W. Jiang, D. Niu, H. Liu, C. Wang, T. Zhao, L. Yin, Y. Shi, B. Chen, Y. Ding, B. Lu, *Adv. Funct. Mater.* **2014**, 24, 7598.
- [100] E. Wang, M. S. Desai, S. W. Lee, *Nano Lett.* **2013**, 13, 2826.
- [101] D.-X. Liu, Y.-L. Sun, W.-F. Dong, R.-Z. Yang, Q.-D. Chen, H.-B. Sun, *Laser Photonics Rev.* **2014**, 8, 882.
- [102] J. Mu, C. Hou, H. Wang, Y. Li, Q. Zhang, M. Zhu, *Sci. Adv.* **2015**, 1, e1500533.
- [103] Q. Shi, J. Li, C. Hou, Y. Shao, Q. Zhang, Y. Li, H. Wang, *Chem. Commun.* **2017**, 53, 11118.
- [104] W. Xu, Z. Qin, C.-T. Chen, H. R. Kwag, Q. Ma, A. Sarkar, M. J. Buehler, D. H. Gracias, *Sci. Adv.* **2017**, 3, e1701084.
- [105] R. R. Nair, P. Blake, A. N. Grigorenko, K. S. Novoselov, T. J. Booth, T. Stauber, N. M. R. Peres, A. K. Geim, *Science* **2008**, 320, 1308.
- [106] J. Liang, Y. Xu, Y. Huang, L. Zhang, Y. Wang, Y. Ma, F. Li, T. Guo, Y. Chen, *J. Phys. Chem. C* **2009**, 113, 9921.
- [107] Y.-L. Zhang, L. Guo, H. Xia, Q.-D. Chen, J. Feng, H.-B. Sun, *Adv. Opt. Mater.* **2014**, 2, 10.
- [108] J. T. Robinson, S. M. Tabakman, Y. Liang, H. Wang, H. S. Casalongue, D. Vinh, H. Dai, *J. Am. Chem. Soc.* **2011**, 133, 6825.
- [109] Y. Jiang, C. Hu, H. Cheng, C. Li, T. Xu, Y. Zhao, H. Shao, L. Qu, *ACS Nano* **2016**, 10, 4735.
- [110] M. Weng, P. Zhou, L. Chen, L. Zhang, W. Zhang, Z. Huang, C. Liu, S. Fan, *Adv. Funct. Mater.* **2016**, 26, 7244.
- [111] M. Qian, Y. S. Zhou, Y. Gao, T. Feng, Z. Sun, L. Jiang, Y. F. Lu, *Appl. Surf. Sci.* **2012**, 258, 9092.
- [112] M. D. Simon, A. K. Geim, *J. Appl. Phys.* **2000**, 87, 6200.
- [113] Y. Su, Z. Xiao, Z. Ye, K. Takahata, *IEEE Electron Device Lett.* **2015**, 36, 393.
- [114] S. Chen, W. Xiong, Y. S. Zhou, Y. F. Lu, X. C. Zeng, *Nanoscale* **2016**, 8, 9746.
- [115] C. Z. Wang, K. M. Ho, *Phys. Rev. Lett.* **1993**, 71, 1184.
- [116] M. Yang, M. Ripoll, *Soft Matter* **2014**, 10, 1006.
- [117] C. Maggi, F. Saglimbeni, M. Dipalo, F. De Angelis, R. Di Leonardo, *Nat. Commun.* **2015**, 6, 7855.
- [118] D. Yoon, Y. W. Son, H. Cheong, *Nano Lett.* **2011**, 11, 3227.
- [119] S. Wang, M. Tambraparni, J. Qiu, J. Tipton, D. Dean, *Macromolecules* **2009**, 42, 5251.
- [120] Z. Zhao, J. Wu, X. Mu, H. Chen, H. J. Qi, D. Fang, *Sci. Adv.* **2017**, 3, e1602326.
- [121] J. Meng, J. Mu, C. Hou, Q. Zhang, Y. Li, H. Wang, *Nanoscale* **2017**, 9, 12963.
- [122] Y. Hu, G. Wu, T. Lan, J. Zhao, Y. Liu, W. Chen, *Adv. Mater.* **2015**, 27, 7867.
- [123] Z. Tang, Z. Gao, S. Jia, F. Wang, Y. Wang, *Adv. Sci.* **2017**, 4, 1600437.
- [124] J. Loomis, P. Xu, B. Panchapakesan, *Nanotechnology* **2013**, 24, 185703.
- [125] H. Arazoe, D. Miyajima, K. Akaike, F. Araoka, E. Sato, T. Hikima, M. Kawamoto, T. Aida, *Nat. Mater.* **2016**, 15, 1084.

- [126] D. D. Han, Y. L. Zhang, H. B. Jiang, H. Xia, J. Feng, Q. D. Chen, H. L. Xu, H. B. Sun, *Adv. Mater.* **2015**, *27*, 332.
- [127] F. Zhao, Y. Zhao, H. Cheng, L. Qu, *Angew. Chem., Int. Ed. Engl.* **2015**, *54*, 14951.
- [128] H. Cheng, Y. Hu, F. Zhao, Z. Dong, Y. Wang, N. Chen, Z. Zhang, L. Qu, *Adv. Mater.* **2014**, *26*, 2909.
- [129] M. Ji, N. Jiang, J. Chang, J. Sun, *Adv. Funct. Mater.* **2014**, *24*, 5412.
- [130] Z. Li, X. Zhang, S. Wang, Y. Yang, B. Qin, K. Wang, T. Xie, Y. Wei, Y. Ji, *Chem. Sci.* **2016**, *7*, 4741.
- [131] L. Chen, M. Weng, P. Zhou, L. Zhang, Z. Huang, W. Zhang, *Nanoscale* **2017**, *9*, 9825.
- [132] J. Abraham, K. S. Vasu, C. D. Williams, K. Gopinadhan, Y. Su, C. T. Cherian, J. Dix, E. Prestat, S. J. Haigh, I. V. Grigorieva, P. Carbone, A. K. Geim, R. R. Nair, *Nat. Nanotechnol.* **2017**, *12*, 546.
- [133] H. Cheng, F. Zhao, J. Xue, G. Shi, L. Jiang, L. Qu, *ACS Nano* **2016**, *10*, 9529.
- [134] Q. Shi, H. Xia, P. Li, Y.-S. Wang, L. Wang, S.-X. Li, G. Wang, C. Lv, L.-G. Niu, H.-B. Sun, *Adv. Opt. Mater.* **2017**, *5*, 1700442.
- [135] J. Peng, D. Zhao, X. Tang, F. Tong, L. Guan, Y. Wang, M. Zhang, T. Cao, *Langmuir* **2013**, *29*, 11809.
- [136] T. Fujigaya, T. Morimoto, Y. Niidome, N. Nakashima, *Adv. Mater.* **2008**, *20*, 3610.
- [137] X. Zhang, C. L. Pint, M. H. Lee, B. E. Schubert, A. Jamshidi, K. Takei, H. Ko, A. Gillies, R. Bardhan, J. J. Urban, M. Wu, R. Fearing, A. Javey, *Nano Lett.* **2011**, *11*, 3239.
- [138] C. Ma, W. Lu, X. Yang, J. He, X. Le, L. Wang, J. Zhang, M. J. Serpe, Y. Huang, T. Chen, *Adv. Funct. Mater.* **2017**, *28*, 1704568.
- [139] D. Kim, H. S. Lee, J. Yoon, *Sci. Rep.* **2016**, *6*, 20921.
- [140] E. Zhang, T. Wang, W. Hong, W. Sun, X. Liu, Z. Tong, *J. Mater. Chem. A* **2014**, *2*, 15633.
- [141] Z. Zhao, H. Wang, L. Shang, Y. Yu, F. Fu, Y. Zhao, Z. Gu, *Adv. Mater.* **2017**, *29*, 1704569.
- [142] H.-B. Jiang, Y.-L. Zhang, Y. Liu, X.-Y. Fu, Y.-F. Li, Y.-Q. Liu, C.-H. Li, H.-B. Sun, *Laser Photonics Rev* **2016**, *10*, 441.
- [143] F. Ge, Y. Zhao, *Chem. Sci.* **2017**, *8*, 6307.
- [144] D. Habault, H. Zhang, Y. Zhao, *Chem. Soc. Rev.* **2013**, *42*, 7244.
- [145] A. Rose, Z. Zhu, C. F. Madigan, T. M. Swager, V. Bulovic, *Nature* **2005**, *434*, 876.
- [146] J. Hu, Y. Zhu, H. Huang, J. Lu, *Prog. Polym. Sci.* **2012**, *37*, 1720.
- [147] A. M. Hubbard, R. W. Mailen, M. A. Zikry, M. D. Dickey, J. Genzer, *Soft Matter* **2017**, *13*, 2299.
- [148] H. Yang, W. R. Leow, T. Wang, J. Wang, J. Yu, K. He, D. Qi, C. Wan, X. Chen, *Adv. Mater.* **2017**, *29*, 1701627.
- [149] L. Yu, Q. Wang, J. Sun, C. Li, C. Zou, Z. He, Z. Wang, L. Zhou, L. Zhang, H. Yang, *J. Mater. Chem. A* **2015**, *3*, 13953.
- [150] S. Iamsaard, S. J. Asshoff, B. Matt, T. Kudernac, J. J. Cornelissen, S. P. Fletcher, N. Katsonis, *Nat. Chem.* **2014**, *6*, 229.
- [151] H. Zeng, O. M. Wani, P. Wasylczyk, R. Kaczmarek, A. Priimagi, *Adv. Mater.* **2017**, *29*, 1701814.
- [152] H. K. Bisoyi, Q. Li, *Chem. Rev.* **2016**, *116*, 15089.
- [153] T. J. White, D. J. Broer, *Nat. Mater.* **2015**, *14*, 1087.
- [154] A. Priimagi, C. J. Barrett, A. Shishido, *J. Mater. Chem. C* **2014**, *2*, 7155.
- [155] M. Yamada, M. Kondo, J. Mamiya, Y. Yu, M. Kinoshita, C. J. Barrett, T. Ikeda, *Angew. Chem., Int. Ed. Engl.* **2008**, *47*, 4986.
- [156] Z. Cheng, T. Wang, X. Li, Y. Zhang, H. Yu, *ACS Appl. Mater. Interfaces* **2015**, *7*, 27494.
- [157] Y. Liu, B. Xu, S. Sun, J. Wei, L. Wu, Y. Yu, *Adv. Mater.* **2017**, *29*, 1604792.
- [158] O. M. Wani, H. Zeng, A. Priimagi, *Nat. Commun.* **2017**, *8*, 15546.
- [159] J. A. Lv, Y. Liu, J. Wei, E. Chen, L. Qin, Y. Yu, *Nature* **2016**, *537*, 179.
- [160] R. R. Kohlmeier, J. Chen, *Angew. Chem., Int. Ed. Engl.* **2013**, *52*, 9234.
- [161] Y. Ji, Y. Y. Huang, R. Rungsawang, E. M. Terentjev, *Adv. Mater.* **2010**, *22*, 3436.
- [162] N. Torras, K. E. Zinoviev, J. E. Marshall, E. M. Terentjev, J. Esteve, *Appl. Phys. Lett.* **2011**, *99*, 254102.
- [163] X. Fan, B. C. King, J. Loomis, E. M. Campo, J. Hegseth, R. W. Cohn, E. Terentjev, B. Panchapakesan, *Nanotechnology* **2014**, *25*, 355501.
- [164] C. J. Camargo, H. Campanella, J. E. Marshall, N. Torras, K. Zinoviev, E. M. Terentjev, J. Esteve, *Macromol. Rapid Commun.* **2011**, *32*, 1953.
- [165] N. Torras, K. E. Zinoviev, C. J. Camargo, E. M. Campo, H. Campanella, J. Esteve, J. E. Marshall, E. M. Terentjev, M. Ormastová, I. Krupa, P. Teplický, B. Mamojka, P. Bruns, B. Roeder, M. Vallribera, R. Malet, S. Zuffanelli, V. Soler, J. Roig, N. Walker, D. Wenn, F. Vossen, F. M. H. Crompvoets, *Sens. Actuators, A* **2014**, *208*, 104.
- [166] Y. Yang, Z. Pei, Z. Li, Y. Wei, Y. Ji, *J. Am. Chem. Soc.* **2016**, *138*, 2118.
- [167] F. Ercole, T. P. Davis, R. A. Evans, *Polym. Chem.* **2010**, *1*, 37.
- [168] Y. Yu, T. Ikeda, *J. Photochem. Photobiol., C* **2004**, *5*, 247.
- [169] Y. L. Yu, M. Nakano, T. Ikeda, *Nature* **2003**, *425*, 145.
- [170] T. Wang, D. Torres, F. E. Fernandez, A. J. Green, C. Wang, N. Sepulveda, *ACS Nano* **2015**, *9*, 4371.
- [171] T. Wang, D. Torres, F. E. Fernandez, C. Wang, N. Sepulveda, *Sci. Adv.* **2017**, *3*, e1602697.
- [172] K. Kumar, C. Knie, D. Bleger, M. A. Peletier, H. Friedrich, S. Hecht, D. J. Broer, M. G. Debije, A. P. Schenning, *Nat. Commun.* **2016**, *7*, 11975.
- [173] W. Wang, Y.-Q. Liu, Y. Liu, B. Han, H. Wang, D.-D. Han, J.-N. Wang, Y.-L. Zhang, H.-B. Sun, *Adv. Funct. Mater.* **2017**, *27*, 1702946.
- [174] X. Han, J. Li, *Chin. Opt. Lett.* **2015**, *13*, 121403.
- [175] M. Kobayashi, J. Abe, *J. Am. Chem. Soc.* **2012**, *134*, 20593.
- [176] D. Jaque, L. Martinez Maestro, B. del Rosal, P. Haro-Gonzalez, A. Benayas, J. L. Plaza, E. Martin Rodriguez, J. Garcia Sole, *Nanoscale* **2014**, *6*, 9494.
- [177] P. K. Jain, X. Huang, I. H. El-Sayed, M. A. El-Sayed, *Acc. Chem. Res.* **2008**, *41*, 1578.
- [178] M. S. Yavuz, Y. Cheng, J. Chen, C. M. Copley, Q. Zhang, M. Rycenga, J. Xie, C. Kim, K. H. Song, A. G. Schwartz, L. V. Wang, Y. Xia, *Nat. Mater.* **2009**, *8*, 935.
- [179] C. Yue, P. Liu, M. Zheng, P. Zhao, Y. Wang, Y. Ma, L. Cai, *Biomaterials* **2013**, *34*, 6853.
- [180] X. Song, Q. Chen, Z. Liu, *Nano Res.* **2014**, *8*, 340.
- [181] L. Hu, S. Gao, X. Ding, D. Wang, J. Jiang, J. Jin, L. Jiang, *ACS Nano* **2015**, *9*, 4835.
- [182] J. Mu, C. Hou, B. Zhu, H. Wang, Y. Li, Q. Zhang, *Sci. Rep.* **2015**, *5*, 9503.
- [183] O. G. Semyonov, *Acta Astronaut.* **2017**, *136*, 190.
- [184] Q. Liao, Z. Liu, W. Liu, C. Deng, N. Yang, *Sci. Rep.* **2015**, *5*, 16543.
- [185] J. N. Coleman, U. Khan, W. J. Blau, Y. K. Gun'ko, *Carbon* **2006**, *44*, 1624.
- [186] A. Peigney, C. Laurent, E. Flahaut, R. R. Bacsa, A. Rousset, *Carbon* **2001**, *39*, 507.
- [187] X. Zhang, L. Song, L. Cai, X. Tian, Q. Zhang, X. Qi, W. Zhou, N. Zhang, F. Yang, Q. Fan, Y. Wang, H. Liu, X. Bai, W. Zhou, S. Xie, *Light: Sci. Appl.* **2015**, *4*, e318.
- [188] B. Xu, F. Wu, F. Wang, S. Chen, G.-P. Cao, Y.-S. Yang, *Chin. J. Chem.* **2006**, *24*, 1505.
- [189] M. F. Yu, O. Lourie, M. J. Dyer, K. Moloni, T. F. Kelly, R. S. Ruoff, *Science* **2000**, *287*, 637.
- [190] Y. Li, K. Wang, J. Wei, Z. Gu, Z. Wang, J. Luo, D. Wu, *Carbon* **2005**, *43*, 31.
- [191] D. J. Babu, M. Lange, G. Cherkashinin, A. Issanin, R. Staudt, J. J. Schneider, *Carbon* **2013**, *61*, 616.
- [192] Y. Zhu, S. Murali, W. Cai, X. Li, J. W. Suk, J. R. Potts, R. S. Ruoff, *Adv. Mater.* **2010**, *22*, 3906.
- [193] Leeladhar, P. Raturi, A. Kumar, J. P. Singh, *Smart Mater. Struct.* **2017**, *26*, 095030.

- [194] D. A. Dikin, S. Stankovich, E. J. Zimney, R. D. Piner, G. H. B. Dommett, G. Evmenenko, S. T. Nguyen, R. S. Ruoff, *Nature* **2007**, *448*, 457.
- [195] Z. L. Hou, W. L. Song, P. Wang, M. J. Meziani, C. Y. Kong, A. Anderson, H. Maimaiti, G. E. LeCroy, H. Qian, Y. P. Sun, *ACS Appl. Mater. Interfaces* **2014**, *6*, 15026.
- [196] P. K. Chow, O. Eksik, N. Koratkar, *Part. Part. Syst. Charact.* **2014**, *31*, 337.
- [197] S. Stankovich, D. A. Dikin, R. D. Piner, K. A. Kohlhaas, A. Kleinhammes, Y. Jia, Y. Wu, S. T. Nguyen, R. S. Ruoff, *Carbon* **2007**, *45*, 1558.
- [198] M. F. El-Kady, V. Strong, S. Dubin, R. B. Kaner, *Science* **2012**, *335*, 1326.
- [199] S. E. Zhu, R. Shabani, J. Rho, Y. Kim, B. H. Hong, J. H. Ahn, H. J. Cho, *Nano Lett.* **2011**, *11*, 977.
- [200] S. Stankovich, D. A. Dikin, G. H. B. Dommett, K. M. Kohlhaas, E. J. Zimney, E. A. Stach, R. D. Piner, S. T. Nguyen, R. S. Ruoff, *Nature* **2006**, *442*, 282.
- [201] M. V. Savos'kin, A. P. Yaroshenko, V. I. Shologon, L. Y. Galushko, *Russ. J. Appl. Chem.* **2004**, *77*, 745.
- [202] B. Liang, J. Lehmann, D. Solomon, J. Kinyangi, J. Grossman, B. O'Neill, J. O. Skjemstad, J. Thies, F. J. Luizão, J. Petersen, E. G. Neves, *Soil Sci. Soc. Am. J.* **2006**, *70*, 1719.
- [203] Y. Tai, G. Lubineau, Z. Yang, *Adv. Mater.* **2016**, *28*, 4665.
- [204] I. Vassalini, I. Alessandri, *Nanoscale* **2017**, *9*, 11446.
- [205] D. Niu, W. Jiang, H. Liu, T. Zhao, B. Lei, Y. Li, L. Yin, Y. Shi, B. Chen, B. Lu, *Sci. Rep.* **2016**, *6*, 27366.
- [206] C.-H. Zhu, Y. Lu, J. Peng, J.-F. Chen, S.-H. Yu, *Adv. Funct. Mater.* **2012**, *22*, 4017.
- [207] L. Yu, H. Yu, *ACS Appl. Mater. Interfaces* **2015**, *7*, 3834.
- [208] H. Lu, Y. Yao, W. M. Huang, J. Leng, D. Hui, *Composites, Part B* **2014**, *62*, 256.
- [209] Y. Feng, M. Qin, H. Guo, K. Yoshino, W. Feng, *ACS Appl. Mater. Interfaces* **2013**, *5*, 10882.
- [210] J. E. Marshall, Y. Ji, N. Torras, K. Zinoviev, E. M. Terentjev, *Soft Matter* **2012**, *8*, 1570.